Variation of Cu, Fe, S and Pb isotopes in sulfides from hydrothermal mineralization from the Yenice region in Çanakkale, Biga Peninsula, NW Turkey

Mustafa Çiçek [a], Tolga Oyman [a], Martin R. Palmer [b]

a *Dokuz Eylül University, Department of Geological Engineering, Buca, İzmir TR-35160, Turkey*

b *University of Southampton, School of Ocean and Earth Science, European Way, Southampton SO14 3ZH, UK*

Abstract

We report the iron (n = 13), copper (n = 13), sulfur (n = 25) and lead (n = 31) isotope compositions of mineralized samples from porphyry, skarn and epithermal mineralization in the Yenice region that lies in the east of the Biga Peninsula, Turkey. The vast majority of isotopic data were analyzed from the world-class Arapuçandere Pb-Zn-Cu (Ag-Au) deposit that is one of the best example of intermediate sulfidation epithermal deposits within the Serbo-Macedonian-Rhodope metallogenic belt in the northeastern of the Aegean. The δ^{56}Fe values range from -1.06 to + 0.46‰ and reflect the complex interplay between redox, Rayleigh and kinetic effects. The δ^{65}Cu values also define a narrow ranges of -0.07 to +0.77‰ that is typical of primary minerals in magmatic-hydrothermal ore deposits worldwide. The Cu isotope values of chalcopyrite from the Arapuçandere deposit tend to progressively increase through the surface, which creates a vector from the proximal to distal portions of magmatic-hydrothermal environment, possibly with local supergene processes within deposit. The sulfides from the Yenice region have a relatively narrow range of δ^{34}S values that range between -4.0 and 3.9‰ and mostly cluster around 0‰, indicating sulfur is mainly derived from a magmatic source at the time of mineralization. All the Pb isotope data that includes results from ore minerals fall

within the fields defined by Oligocene to Miocene Aegean-West Anatolian magmatic rocks. This observation supports the hypothesis that the metals and sulfur contained within all the various styles of mineralization considered here were derived entirely from these granitoids, with no significant contamination from the local basement rocks. This observation also constrains the processes controlling the Fe and Cu isotope compositions to those operating within the porphyry, skarn, and epithermal hydrothermal systems, rather than contamination by interaction with the basement rocks.

1. Introduction

Transition metal isotopes are increasingly being used to constrain the sources of metal and improve the understanding of ore-forming processes because they may provide more direct evidence for tracing spatial and temporal zoning patterns of metal transport and deposition in ore deposits than traditional H, O, and C stable isotopes studies alone (Yao et al., 2016; Zhu et al., 2016; Wang et al., 2017; Mathur and Wang, 2019). The magmatic-hydrothermal systems contain fluids with significant concentrations of sulfur, and therefore S isotopes have been widely used to provide information about the origin of the S source and metal mobility in ore-forming environments (Rye, 2005; Seal, 2006; Hutchison et al., 2020). Further, copper and iron are two of the most commonly used transition metal isotopes applied to porphyry and skarn deposits (Maher and Larson, 2007; Mathur et al., 2013; Mirnejad et al., 2010; Li et al., 2010, 2016; Palacios et al., 2011; Wang et al., 2011; Zhu et al., 2016; Gregory and Mathur, 2017; Wawryk and Foden, 2017; He et al., 2020), and epithermal and polymetallic deposits (Markl et al., 2006a, 2006b; Saunders et al., 2016; Duan et al., 2016; Wang et al., 2017; Wu et al., 2017).

Sulfides from magmatic-hydrothermal ore deposits generally show a narrow range of δ^{65}Cu values between -1 and +1‰ (clustering around 0‰), whereas minerals from leached

caps show lighter δ^{65}Cu values (mostly < -1‰), and supergene enrichment zones display a wider range in δ^{65}Cu values generally > +1‰ (e.g., Mathur et al., 2009, 2012; Mirnejad et al., 2010; Duan et al., 2016; Mathur and Wang, 2019). Fe isotope variations of Fe-bearing minerals from magmatic-hydrothermal deposits are largely controlled by the δ^{56}Fe of the ore-forming fluid and sulfide formation processes, and mostly range from -2 to +1‰ (Li et al., 2010; Wang et al., 2011, 2015; Zhu et al., 2018). More recently, He et al. (2020) determined distinct Fe isotopic signatures in disseminated and vein-type pyrite in a porphyry Cu-Mo system (Tongshankou, Eastern China), in which the granodiorite porphyries display a small δ^{56}Fe variation (0.00 to +0.17‰). In comparison, disseminated pyrites in the hydrothermally altered zone had relatively high δ^{56}Fe values of +0.14 to +0.40‰, and pyrites from the veins had more variable Fe isotope compositions (-0.48 to 0.34‰), that likely reflect Rayleigh effects during sulfide precipitation. Ore deposits in the Biga Peninsula have not received sufficient attention regard to copper and iron isotopes. Only a few studies have attempted to report a detailed traditional (i.e., H, O, S) and radiogenic Pb isotope compositions from Koru (Bozkaya and Gökçe, 2009; Çiçek et al., 2012; Çiçek and Oyman, 2016; Bozkaya et al., 2020), Şahinli/Tesbihdere (Yılmaz et al., 2010; Bozkaya et al., 2014; Çiçek and Oyman, 2016), Arapuçandere (Bozkaya et al., 2008; Bozkaya, 2011; Bozkaya and Banks, 2015), Kalkım (Akıska et al., 2013), Çataltepe (Demirela, 2011), Madendağ and Kartadağ (Ünal-İmer et al., 2013) deposits in the Biga Peninsula.

The Yenice ore district covers ~70 km^2 (Fig. 1) and hosts a variety of mineralization; including Mo ± Cu porphyry, Fe ± Cu proximal and Pb- Zn-Cu distal skarn, and Pb-Zn-Cu ± Ag ± Au epithermal mineralization (Çiçek et al., 2017a, 2017b). Early contributions (Yücelay, 1971, 1976; Atılgan, 1977; Yenigün, 1978; Çağatay, 1980) focused on the geological mapping, and partly described the mineralogical characteristics of Arapuçandere, Alandere, and Kozcağız (Sofular) mineralization. Among these mineralization, Arapuçandere is the only

deposit where scientific studies with advanced methods (including O, H, S and Pb isotopes, crushed leach studies of fluid inclusions) have been conducted to date (Orgün et al., 2005; Bozkaya et al., 2008; Bozkaya, 2011; 2015). Nevertheless, it is still not clear yet whether the source of metals in mineralization was derived from the host rocks (Anıl, 1979, 1984; Çağatay, 1980; Anıl and Yaman, 1985; Bozkaya, 2011) or Cenozoic magmatism (Yücelay, 1971, 1976; Orgün et al., 2005; Bozkaya and Banks, 2015) in the Yenice region.

Here, we report the results of an Fe, Cu and S study of mineralization in the Yenice region of the Biga Peninsula, Turkey. This comprehensive data set is used to explain the metal source and the evolution of a possible ore-forming fluid during the formation of the magmatic-hydrothermal systems in the region, especially for the Arapuçandere deposit. We also report Pb isotope data of sulfides from ore-zones and local granitoids to further constrain potential relationships between mineralization and local magmatism, and to supplement previously published Pb isotope data from the Koru (Bozkaya and Gökçe, 2009; Çiçek and Oyman, 2016), Tesbihdere (Çiçek and Oyman, 2016), Arapuçandere (Bozkaya, 2011) and Kalkım (Akıska et al., 2013) deposits. Finally, the results obtained from this study can be used as a guide to evaluating the importance of the region in future mineral explorations.

2. Regional Geology

The Neotethyan orogen is marked by a major porphyry-related mineralized zone that extends across central and southeast Europe, Turkey, and Iran through the Himalayan region to Indochina, and is one of the world's largest metallogenic belts (Richards, 2015). The Biga Peninsula is a part of the Serbo-Macedonian-Rhodope metallogenic belt in the Balkans, which is essentially the eastward continuation of this orogenic belt in the northeastern of the Aegean region, and hosts numerous world-class porphyry, epithermal, and skarn deposits (e.g., Yiğit, 2012; Richards, 2015; Sánchez et al., 2016; Menant et al., 2018; Kuşcu et al., 2019). Although

the western segment is highly prospective and has been extensively explored, the east of the Biga Peninsula (which includes the Yenice region) has received less attention (Fig. 1).

Two major geodynamic events that shaped the Biga Peninsula are the pre-Cenozoic amalgamation and the Cenozoic crustal extension during the consumption of the Tethys oceans (e.g., Şengör and Yılmaz, 1981; Okay et al., 1996; Bozkurt, 2001; Richards, 2015). The amalgamation of several continental fragments (i.e., Gondwana and Laurasia) commenced during the subduction and closure of the Paleotethys in the Late Triassic-Early Jurassic, and the opening of the Neotethyan ocean in the Permian-Early Triassic (Stampfli and Borel, 2004; Moix et al., 2008). The İzmir-Ankara-Erzincan (IAE) suture zone developed in response to the Late Mesozoic northward subduction of the northern branch of the Neotethys below the accretionary Laurasian margin and the continental collision between the Gondwana and Laurasia continents in the Late Cretaceous-Eocene (Şengör and Yılmaz, 1981). Following Late Cretaceous subduction of the Vardar and İzmir-Ankara-Erzincan oceans (Georgiev et al., 2012; Gülmez et al., 2016), syn- to post-collisional magmatic belts developed in the Middle Eocene (e.g., Altunkaynak et al., 2012a; Ersoy and Palmer, 2013; Aysal, 2015; Ersoy et al., 2017). The IAE suture zone separates the Sakarya Zone from the Anatolide- Tauride Platform in the south, and the Intra-Pontide suture tectonically separates the Sakarya zone from the Istanbul blocks in the north (Şengör and Yılmaz, 1981; Okay et al., 1996). The Yenice region, which is the subject of this study, is located in the Sakarya zone in the east of the Biga Peninsula.

The pre-Cenozoic basement rocks of the Sakarya Zone in the Biga Peninsula are characterized by metamorphic rocks of the Kazdağ massif metamorphic core complex and metamorphic/non-metamorphic rocks of the Karakaya Complex (Duru et al., 2004; Okay and Göncüoğlu, 2004). Kazdağ massif is composed of the gneisses, amphibolites, marbles, high-grade schists, and metaophiolites, which is tectonically overlain by the Permian-Triassic

orogenic series and Paleotethys subduction-accretion units of the Karakaya Complex (Şengör et al., 1984; Okay et al., 1991; Picket and Robertson, 1996). The Karakaya Complex is subdivided into two groups as (see Okay and Göncüoğlu, 2004 and references therein): (1) a tectonic melange with blocks of metabasic rocks, metacarbonates, meta-arenites and metapelites as Lower Karakaya Complex (i.e., Nilüfer Unit), and (2) strongly deformed Permian-Triassic clastic and volcano-sedimentary units with limestone blocks as Upper Karakaya Complex (i.e., Hodul and Çal Units, Orhanlar Greywacke, Akgöl Formation). The regional NE-directed extension since the earliest Eocene (Beccaletto et al., 2005) led to exhumation of the Kazdağ Massif and the emplacement of Evciler pluton during the Late Oligocene-Early Miocene (Okay and Satır, 2000; Cavazza et al., 2009; Altunkaynak et al., 2012b).

Hydrothermal systems in the region (i.e., porphyry and epithermal deposits) are spatially and temporally associated with the development of the Cenozoic volcanic activity (Yiğit, 2012; Kuşcu et al., 2019). The Cenozoic volcanism in the Biga Peninsula is characterized by extensive post-collisional volcanic associations developed interruptedly between ~43 and 15 Ma (i.e., from the Middle Eocene to Upper Miocene) (Ersoy et al., 2017). Collectively, the volcanic rocks associations in the Biga Peninsula comprise; (1) the Middle-Upper Eocene Balıklıçeşme volcanics, (2) the Lower-Upper Oligocene Kirazlı volcanics, (3) the Upper Oligocene Hallaçlar volcanics, (4) the Lower-Middle Miocene Dedetepe volcanics and Ezine-Ayvacık volcanics, and (5) the Upper Miocene Taştepe volcanics (Fig. 1) (Ersoy et al., 2017 and references therein). The Middle Eocene to Middle Miocene volcanic units have a subduction-related calc-alkalic to shoshonitic geochemical signature. (e.g., Krushensky, 1976; Ercan et al., 1995, 1998; Aldanmaz et al., 2000; Altunkaynak et al., 2012a, 2012b; Genç et al., 2012; Akal, 2013; Gülmez et al., 2013). The last phase of the Cenozoic volcanic activity

is represented by Na-alkaline Taştepe basalts as a result of advanced stages of crustal extension in the late Miocene (Aldanmaz et al., 2000; Altunkaynak and Genç, 2008).

The Bayramiç formation, consisting of Plio-Quaternary fluvial (sandstone, conglomerate and shale) and lacustrine (carbonates) sediments, unconformably covers all units in the central Biga Peninsula (Siyako et al., 1989).

3. Local Geology

The Yenice region contains extensive calc-alkaline Cenozoic magmatic rocks related to the regional collisional and post-collisional tectonic regime (Aysal, 2015; Çiçek et al., 2017b). The basement rocks around the region are comprised of the Permo-Triassic Karakaya Complex, including Nilüfer and Hodul Units and numerous exhumed igneous bodies and coeval volcanic rocks (Figs. 2 and 3). The Nilüfer unit, which constitutes the Lower Karakaya Complex, consists of highly deformed schist, phyllite and carbonate series that have been affected by high pressure and low-temperature metamorphism (Okay and Göncüoğlu, 2004). The Hodul unit of the Upper Karakaya Complex is made up of a variably deformed Triassic clastic series. In the Yenice region, these series are mainly composed of arkosic sandstones intercalated with pelitic rocks, which pass upward into greywacke and shales with blocks of diabase and Permian limestone. The Hodul unit unconformably overlies metamorphic basement rocks of the Nilüfer unit.

Granitoids in the north of Yenice include the Nevruz, Çakıroba, Soğucak and Sofular plutons exposed over ~15 km^2 with a segmented distribution along a NE-SW direction (Fig. 2). In the study area, deep-seated plutons (e.g., Nevruz-Çakıroba intrusions), subvolcanic facies (e.g. Soğucak intrusion) and volcanic rocks (e.g., Hallaçlar volcanics) cover a wide area (Çiçek et al., 2017b). Previously reported geochronological data (e.g., K-Ar and U-Pb ages) range from 18.8 ± 1.3 to 27.4 ± 1.8 Ma for the granitoid intrusions (Karacık et al., 2008;

Delaloye and Bingöl, 2000; Aysal, 2015; Çiçek et al., 2017b), indicating that the plutons were intruded and cooled during the Late Oligocene to Early Miocene. Contacts between the granitoids and the basement rocks are observed in many places, together with varying degrees of contact metamorphism. For example, there is well-developed contact metamorphism between the Nevruz-Çakıroba stock and the basement Hodul unit that is indicative of the potential for skarn-type mineralization. The Çakıroba porphyry is located in the highest elevation (max, 700 m above sea level) in the NE of the stock, and porphyritic textures and intense alteration are observed in its upper elevations. The Sofular intrusion is located in the northwest of the study area, where it forms two separate NE-SW trending outcrops with a combined area of 1.5 km^2. The intrusion has a holocrystalline texture, similar to other intrusions in the south. The intrusion is topographically emplaced into higher elevations and contains coarse-grained phenocrysts (up to 5 mm) towards the north. The Soğucak pluton is located in the northeast of the study area, and is likely a major source of porphyry, skarn and hydrothermal mineralization in the region.

The volcanic rocks, known as the Hallaçlar volcanics in the Biga Peninsula (Dönmez et al., 2005), widely crop out around the Arapuçandere deposit in the eastern part of the Yenice region and comprise highly altered andesite, basaltic andesite lavas and pyroclastic rocks. The andesitic-dacitic rocks from the Hallaçlar volcanics yielded K/Ar and U-Pb zircon ages ranging from 28 to 23 Ma (Krushensky, 1976; Dayal, 1984; Ağdemir et al., 1994; Altunkaynak and Genç, 2008; Genç et al., 2012; Ersoy et al., 2017). The volcanic activity of this unit is thought to have continued from the Late Oligocene to the Early Miocene (Genç et al., 2012). In the south, all basement and magmatic-volcanic units are unconformably covered by Quaternary alluvium and coeval terrace sediments with unconsolidated clastic sediments (i.e., gravel, sand, silt and clay). The deposition of these sediments is controlled by structure related to NE trending strike-slip Yenice-Gönen fault zone (Fig. 2).

4. Characteristics of the mineralization in the Yenice region

The mineralization in the Yenice region, from south to north, comprise Alandere Pb-Zn-Cu distal skarn, Alankaya Fe ± Cu proximal skarn, Arapuçandere Pb-Zn-Cu (Ag-Au) epithermal veins, Soğucak Mo- Cu porphyry and Fe ± Cu skarn, Tepetarla Pb-Zn mineralization, Sofular intraplutonic Cu veinlets, Kozcağız-I Pb-Zn-Cu epithermal vein and Kozcağız-II Pb-Zn skarn (Fig. 2). Soğucak pluton is one of the most important sources for the studied mineralization in the northeast of the Yenice region and drill core samples recovered by the Esan Company reveal the presence of mineralized quartz veinlets with a thickness of ~1 cm in the stockwork type Mo-Cu mineralization (Fig. 3A). Among these mineralization in the Yenice region, the Arapuçandere mine is the only ore deposit that is now being actively operated by the Nesco Mining Company (Fig. 3B). The deposit has reserves of 4 million tonnes (Mt) ore at an average grade of 16.4% Pb, 12.1% Zn, 2.2% Cu, 260 g/t Ag and 4 g/t Au, and is the most economically important Pb-Zn-Cu ± Ag ± Au deposit in the Biga Peninsula (MTA, 1993a, 1993b).

The Arapuçandere Pb-Zn-Cu (Ag-Au) veins were discovered in the early 1970s during regional exploration carried out by MTA (Mineral Research and Exploration Institute of Turkey) and five economic hydrothermal veins were identified as I to V veins (Fig. 3B). The first mining operations started in the early1980s, but the I-II-III veins were closed as they were uneconomic. The IV and V veins are still actively exploited. These two vein systems show a close genetic relationship as suggested by their temporal and spatial association. Both veins show W-E strike with steep dips 70◦ to 80◦S at the surface. The dips of the veins decrease (~40-50^{o}S) downward and link at an elevation of 120 m above sea level (asl). The principal ore paragenesis within the veins displays a similar assemblage, consisting of galena, sphalerite, chalcopyrite, pyrite, magnetite, Ag-sulfosalts, and Ag-rich fahlores and minor amounts of Fe- and Co-rich sulfarsenides, and Au (in order of decreasing abundance) (Fig. 4A, B and C).

Hematite, goethite, and chalcocite-covellite are secondary phases resulting from supergene alteration. Major gangue minerals in both veins exhibit a zonation pattern represented by a decrease in quartz and an increase in calcite with locally minor barite towards deeper levels of the deposit**.**

The Soğucak pluton contains quartz-dominated veinlets of molybdenite, pyrite and chalcopyrite that are restricted to the porphyritic subvolcanic part of the pluton that is altered to phyllic to propylitic assemblages (Fig. 3A). The inner propylitic alteration at Soğucak formed as a prograde and transitional alteration zone that passes downwards into the potassic alteration in the deeper parts of the porphyry. The ore paragenesis of these veinlets is dominated by fine-grained molybdenite, pyrite, bornite, enargite, sphalerite, and chalcopyrite (Fig. 4D). Primary copper sulfides are occasionally replaced by secondary chalcocite and covellite. The western part of the Soğucak porphyry contains skarn zones with high Fe (±Cu) concentrations which formed by the metasomatism of carbonate lenses and intercalations within the clastic rocks of the Hodul unit by magmatic fluids (Çiçek and Oyman, 2019a). The endoskarn of the Soğucak Fe (±Cu) skarn is composed of pyroxene, epidote, chlorite and lesser amounts of disseminated chalcopyrite and pyrite in a zone up to ~2 m thick. The exoskarn zones are up to ~50 m thick, and contain predominantly Fe with lesser amounts of Cu. They developed through selective metasomatism by diffusion and infiltration via circulating hydrothermal fluids into the Hodul unit. The skarn mineralization in this proximal zone is composed of magnetite, pyrite, ilmenite and minor pyrrhotite, hematite, goethite, maghemite, and lepidocrocite (Fig. 4E). The outermost parts of the system are characterized by tremolite-actinolite bearing calc-silicate hornfels with disseminated pyrite and magnetite.

In the southwest of the region, the Alandere orebody is distributed in veins, with mineral zoning controlled by carbonate lenses of the Hodul unit. The skarn silicates mainly comprise tremolite-actinolite, garnet and clinopyroxene. Hornblende-hornfels facies lie within

the outer aureoles of the distal skarn zone where the skarn passes into clastic sandstone. The primary ore paragenesis of the Alandere distal skarn consists of galena, sphalerite, chalcopyrite, pyrite, hematite and lillianite (Fig. 4F). Magnetite is also present, together with secondary goethite and chalcocite-covellite. The Alankaya proximal skarn lies within the Hodul unit, and includes two irregular massive Fe ± Cu ore bodies that lack any visible contact with the porphyry masses. However, the wide area of hornblende-hornfels facies around the skarn suggests an intrusion lies close to the surface. The Alankaya mineralization is a calcic-type skarn, consisting predominately of garnet and clinopyroxene, with lesser amphibole and epidote. Magnetite is the predominant ore mineral, followed by chalcopyrite, hematite and pyrrhotite. The Alandere Pb-Zn-Cu mineralization is a distal skarn, located south of the Çakıroba granitoid. Here, NE-SW and NW-SE oriented fracture systems formed pathways for the movement of magmatic-hydrothermal fluids within the clastic sediments of the Hodul unit.

In the northern of the region, the quartz vein and associated stockwork-type Cu veinlets at Sofular were emplaced into the Sofular intrusion, which strikes N25◦E with dips 80ºNW. This mineralized vein has an average width of 0.5–1 m and has been traced at the surface for ~10 m along strike where the ore assemblage is represented mainly by chalcopyrite with lesser amounts of chalcocite-covellite, and malachite as secondary Cu minerals. The Tepetarla Pb-Zn mineralization is hosted by the schists of the Nilüfer unit between the NE-SW trending two-part Sofular intrusion. The mineralization is present as small nodules comprising mainly coarse-grained galena with lesser amount of sphalerite, chalcopyrite and lead oxides (i.e., massicot and minium). The Kozcağız-I and Kozcağız-II mineralization were emplaced into a N75ºE trending fault zone and the Pb-Zn-Cu base metals were exploited in the 1970's. The Kozcağız-I Pb-Zn-Cu epithermal mineralization is hosted by sedimentary rocks of the Hodul unit and consists of N80ºW trending vein swarm with dips 75º to 85ºNE. The ore assemblage is composed mainly of galena, chalcopyrite and sphalerite with a lesser amount of arsenopyrite

and pyrite (Fig. 4G, H). The principal gangue mineral is coarse-grained quartz, with less abundant calcite. Kozcağız-II is located 1 km east of the Kozcağız-I mineralization and contains Pb-Zn (Cu) skarn type mineralization hosted by locally hornfels rocks within the sedimentary rocks of the Hodul unit. Euhedral crystals of galena and sphalerite are present as disseminated ore within stockwork-type irregular quartz veinlets in the hornfels (Fig. 4I).

5. Sampling and analytical methods

5.1. Sampling strategy

Field observations and samples for isotope analysis were mainly taken from the Arapuçandere deposit and the Soğucak porphyry-skarn. Representative samples from the Soğucak area were collected from the surface so as to intersect the different types of hydrothermal alteration across the porphyry and skarn zonation. All samples from the Arapuçandere deposit were taken from the five different underground mining levels of the deposit (elevations of 308, 275, 240, 200 and 160 m above sea level (asl)) that intersect veins IV and V. A mineralized vein sample was also selected from vein II from the surface at an elevation of 425 m asl. Other mineralization sites within the Yenice region, which present substantial differences in term of the location, ore formation styles and paragenesis, are mostly exposed in a limited area. Hence, a small number of samples were taken from surface outcrops representing the dominant styles of mineralization. Detailed descriptions of the samples that were analyzed in this study are given in Table 1.

5.2. Analytical methods

Polished thin sections from the ore bodies were examined to determine the different phases of mineralization. Samples were then chosen to avoid ore mineral intergrowths or overgrowths which may be products of reactions of primary sulfides with later fluids, especially for galena-chalcopyrite mineral pairs. Samples were crushed in a jaw crusher that

was rinsed with ethanol between samples. Mineral grains, without visible impurities, were then handpicked under a binocular microscope. Different types of sulfides have been analyzed for isotopic compositions due to the differences in ore paragenesis of mineralization in some locations.

Thirteen samples were analyzed for Fe and Cu isotope ratios. The purification, and determination of the Cu and Fe isotopic compositions of chalcopyrite and pyrite were performed at Queen's Facility for Isotope Research (QFIR), Queen's University, Canada. A chromatographic procedure was performed on all samples by following the preparation, digestion, and chemical separation protocols without pre-purification developed by Kidder et al. (2020) to isolate Fe and Cu, prior to measurement. Details on the instrumentation and analytical procedure can be found in Kidder et al. (2020). Briefly, approximately 1–100 mg of the selected sulfide grains (i.e., chalcopyrite and pyrite) were digested using a mixture of concentrated HF, HNO_3 and HCI. Following complete digestion, the Cu and Fe were purified on a chromatographic column using AG MP-1 M resin (Bio-Rad California, 100–200 mesh) to isolate Fe and Cu from each other and other matrix elements. The chromatographic purification method was based on a procedure modified from Maréchal et al. (1999) and Borrok et al. (2008). Remnant matrix elements were eluted using 4 mL of 9 M HCI. Copper was collected using 15 mL of 5 M HCl and iron was then collected in the following 5 mL of 1 M HCl. At the end of the chromatographic elution, recovery and purity of Fe and Cu were close to 100% and the total procedural blanks were <20 ng for Fe and <200 pg for Cu, which is negligible relative to the total amounts of Fe and Cu in samples.

The Fe and Cu isotope measurements were performed on a Thermo Finnigan NeptuneTM Series Multi-collector inductively coupled plasma mass spectrometry (MC-ICP-MS) using standard-sample bracketing with IRMM-014 (Taylor et al., 1992) and ERM-AE633 (Moeller et al., 2012) reference materials for instrumental mass bias correction factors of Fe

and Cu, respectively. The commonly used reference material IRMM-014 Iron isotope compositions are reported in per mil deviation $\delta^{56}Fe$ and $\delta^{57}Fe$ relative to the certified standard IRMM-014, defined as $\delta^{x}Fe = [(\delta^{x}Fe/^{54}Fe)_{sample}/(\delta^{x}Fe/^{54}Fe)_{IRMM\text{-}014} - 1] * 10^{3}$, where × is either 57 or 56 (Baxter et al., 2006). Copper isotope compositions are reported in per mil deviation $\delta^{65}Cu$ relative to the certified standard substance ERM-AE633, defined as $\delta^{65}Cu = [(\delta^{65}Cu/^{63}Cu)_{sample}/(\delta^{65}Cu/^{63}Cu)_{ERM633} - 1] * 10^{3}$ (Baxter et al., 2006). The majority of published Cu isotope data are reported relative to the reference material NIST SRM 976 (Moeller et al., 2012; Mathur and Wang, 2019). This standard is no longer available being supplied by the National Institute of Standards and Technology (NIST). Moeller et al. (2012) developed the new reference material ERM-AE633 relative to the commonly used this standard and the Cu isotope amount ratio of NIST SRM 976 yielded $\delta^{65}Cu$ value of –0.01 ± 0.05‰ relative to ERM-AE633. Hence, Cu isotope data in this study do not need to be converted to $\delta^{65}Cu$ values relative to NIST SRM 976 standard (Mathur and Wang, 2019). Certified reference materials (CRM) of CCU-1c and PTC-1 obtained from the Canadian Certified references materials Project (CCRMP) were measured along with the samples to ensure quality assurance and quality control. The 2σ error for the variations of the standards for nine analytical sessions was observed to be ± 0.17‰ for $\delta^{65}Cu$, ±0.12‰ for $\delta^{57}Fe$ and ± 0.06‰ for $\delta^{56}Fe$.

Sulfur isotope compositions were determined from 25 mineral grains from various types of mineralization in the Yenice region. Samples for S isotope analyses were weighed into tin capsules and the sulfur isotopic composition measured using a Finnigan MAT 253 stable isotope ratio mass spectrometer system coupled to a Costech ECS 4010 elemental analyzer, at the Queen's Facility for Isotope Research (QFIR), Queen's University, Canada. Sulfur in sulfide was converted to SO_2 by reacting the sulfide with Cu_2O using a continuous flow device, and then the S isotope ratios were analyzed using the mass spectrometer. $\delta^{34}S$ values were calculated by normalizing the $^{34}S/^{32}S$ ratios in the sample to that in the Vienna Canyon Diablo

Troilite (VCDT) international standard, values are reported using the delta (δ) notation in units of per mil (‰) and are reproducible to ± 0.2 per mil (±2σ).

Lead isotope ratios were measured on 27 grains of galena, pyrite, chalcopyrite, and magnetite from the various types of mineralization in the Yenice region. Whole-rock Pb isotope analyses were also performed on the four freshest porphyry samples selected from So˘gucak. Pb isotopic compositions of minerals and whole rocks were performed at the University of Southampton, United Kingdom. The analytical procedure involved dissolution of sample using HF and HNO_3 in vials, followed by the Pb separation and purification using AG1x8 anion exchange resin. The analyses were performed using a VG Sector 54 thermal ionization mass spectrometer and MC-ICP-MS (Neptune). Both TIMS and MC-ICP-MS techniques used the double spike technique to correct instrumental bias (Ishizuka et al., 2003). The NBS-981 standard was used to calibrate the analytical results. Long-term repeated measurement values (n = 7) for NBS-981 standard are as follows: $^{206}Pb/^{204}Pb$ = 19.9416 ± 0.0033, $^{207}Pb/^{204}Pb$ = 15.4981 ± 0.0020, and $^{208}Pb/^{204}Pb$ = 36.7166 ± 0.0073 (±2σ).

6. Results

6.1. Cu isotopes

The overall $\delta^{65}Cu$ isotope range measured from the Yenice region is between – 0.07 and + 0.77‰ (Table 2), which is typical of mineralized systems with Cu isotopic compositions near 0‰ that have not been influenced by low-temperature redox processes (Mathur et al., 2009). Two pyrite samples from the inner pyropylitic and phyllic alteration zones of the Soğucak porphyry display a wide range between + 0.13 to + 0.77‰, respectively, with a pyrite sample from the Soğucak Fe ± Cu skarn has an intermediate value of + 0.52‰. The $\delta^{65}Cu$ values from the II-, IV- and V-veins in Arapuçandere deposit range from – 0.05 to +0.46‰, with an average of +0.25‰. The surface sample from the II-vein in the Arapuçandere deposit

has a δ^{65}Cu value of +0.18‰, compared to +0.13 and + 0.35‰ in the upper and middle levels of the IV vein, respectively, and – 0.05‰ in the sample from the deeper level. In contrast, the highest δ^{65}Cu value in the V-vein was obtained from the deepest level (+0.46‰), compared to δ^{65}Cu values of +0.25 and +0.39‰ in samples from the middle and upper levels, respectively. The δ^{65}Cu values of chalcopyrite samples from the other mineralization in Yenice region are – 0.07‰ for the Kozcağız-I Pb-Zn-Cu epithermal vein, +0.12‰ for Cu-rich mineralized quartz veins in Sofular intrusion and +0.16‰ for Alandere Pb-Zn-Cu distal skarn.

6.2. Fe isotopes

The δ^{56}Fe values of sulfides from the Yenice region range from – 1.06 to + 0.46‰ (Table 2). The Soğucak porphyry alteration and skarn have the highest δ^{56}Fe values in the study area, with δ^{56}Fe values for disseminated pyrite samples from the inner pyropylitic and phyllic alteration zones of + 0.44 and + 0.46‰, respectively, whereas the massive pyrite sample from the skarn has δ^{56}Fe value of + 0.17‰. The samples from Arapuçandere have a narrow range of δ^{56}Fe values from – 0.73 to – 0.43‰. The highest δ^{56}Fe value of – 0.43‰ was obtained from the surface sample of II-vein in the north of the mine. The δ^{56}Fe values in the IV-vein varies from – 0.68‰ in the deepest level to – 0.57‰ in the uppermost levels, with the sample from the middle level having the highest δ^{56}Fe value of – 0.47‰. The sample from the deepest level of the V-vein has the lowest δ^{56}Fe value (– 0.73‰) and the two samples from the middle and upper levels gave δ^{56}Fe values of – 0.64‰ and – 0.52‰, respectively. In comparison, the Cu-rich mineralized quartz veins in Sofular intrusion has a δ^{56}Fe value of – 0.06‰; intermediate between the samples from the Soğucak skarn and the veins in the Arapuçandere deposit. Finally, the samples from the Alandere Pb-Zn-Cu distal skarn (– 1.06‰) and the Kozcağız-I Pb-Zn-Cu epithermal vein (– 1.02‰) have the lowest δ^{56}Fe values in the Yenice region.

6.3. S isotopes

The sulfur isotopic results of galena, sphalerite, chalcopyrite, and pyrite from the various types of mineralization in the Yenice region are given in Table 3. The overall $\delta^{34}S$ values of sulfides range from – 4.0‰ to + 3.9‰, which are remarkably clustered around typical magmatic values of 0 ± 5‰ (e.g., Chaussidon et al., 1989; Labidi et al., 2012, 2013, 2015; Hutchison et al., 2020). The highest $\delta^{34}S$ value of + 3.9‰ was obtained from a disseminated pyrite sample from the inner pyropylitic zone of the Soğucak porphyry. The $\delta^{34}S$ values of two massive pyrite samples from the Soğucak skarn range between +2.3 to +3.3‰. The sulfides from the Arapuçandere deposit have an average $\delta^{34}S$ value of – 1.3‰ that range between – 4.0 to +0.3‰, with the only positive $\delta^{34}S$ value of +0.6‰ for a sphalerite sample from II to vein, whereas IV and V veins exhibit a negative range of $\delta^{34}S$ values for galena, sphalerite, and chalcopyrite samples ranging from – 4.0 to – 1.2‰, – 1.8 to – 0.3‰, and – 0.9 to – 0.6‰, respectively. Collectively, the Arapuçandere deposit has a narrow and homogeneous range of $\delta^{34}S$ values for sulfides.

Sulfides from the other mineralization in the northern part of the region have variable sulfur isotopic compositions with $\delta^{34}S$ ranging from – 3.1 to + 2.2‰. Chalcopyrite sample from Cu-rich mineralized quartz veins from the Sofular intrusion has a $\delta^{34}S$ value of + 2.2‰. Sulfides samples from Kozcağız-I Pb-Zn-Cu epithermal vein exhibit a limited sulfur isotopic compositional variety with $\delta^{34}S$ values of – 0.6‰ for galena, 0.6‰ for sphalerite, and 0.8‰ for chalcopyrite. Two galena samples from Kozcağız II Pb-Zn (Cu) skarn type mineralization and Tepetarla Pb-Zn mineralization have similar negative sulfur isotopic compositions with $\delta^{34}S$ values of – 2.7‰ and – 3.1‰, respectively. In the southwestern part of the region, the $\delta^{34}S$ values of sulfides from the Alandere Pb-Zn-Cu distal skarn range between – 1.8 to + 0.1‰.

6.4. Pb isotopes

Pb isotope data of galena, pyrite, chalcopyrite and magnetite from the entire Yenice region shows a narrow range in isotopic ratios. Overall, the sulfide samples have relatively

homogeneous Pb isotope compositions with $^{206}Pb/^{204}Pb$, $^{207}Pb/^{204}Pb$, and $^{208}Pb/^{204}Pb$ values ranging from 18.7626 to 18.7776, 15.6886 to 15.6994 and 38.9305 to 38.9700, respectively (Table 4). In detail, the galena samples from the IV and V veins at the Arapuçandere deposit show very similar Pb isotope values, with $^{206}Pb/^{204}Pb$ ratios of 18.7626 to 18.7776, $^{207}Pb/^{204}Pb$ ratios of 15.6909 to 15.6994, and $^{208}Pb/^{204}Pb$ ratios of 38.9343 to 38.9700. The $^{206}Pb/^{204}Pb$, $^{207}Pb/^{204}Pb$ and $^{208}Pb/^{204}Pb$ ratios of whole-rock samples from Soğucak porphyry show ranges of 18.8412 to 18.8669, 15.7015 to 15.7041 and 38.9984 to 39.0045, respectively. The Pb isotope ratios of sulfides from other mineralization zones in the region are within the range seen in the Arapuçandere deposit, except for the Alankaya Fe skarn. All the sulfides samples plot above the upper crust evolution curve of Zartman and Doe (1981).

7. Discussion

7.1. Ore-Forming fluid evolution at northeast Yenice region

7.1.1. Cu isotopic zonation

Magmatic-hydrothermal systems associated with porphyry intrusions can generate Cu isotope variations in primary high-temperature sulfides, and in secondary low-temperature sulfides and oxides (Maher and Larson, 2007; Li et al., 2010; Braxton and Mathur, 2011; Palacios et al., 2011; Mathur et al., 2009, 2012; Yao et al., 2016; Mathur and Wang, 2019). Hence, Cu isotope studies may provide a mechanism for tracing the spatial and temporal zoning patterns of Cu transport and deposition in magmatic-hydrothermal deposits (Larson et al., 2003; Graham et al., 2004).

The $\delta^{65}Cu$ values of the sulfides in the Yenice region analyzed in this study (– 0.07 to +0.77‰) are typical of the Cu isotopic signatures of primary sulfides in magmatic-hydrothermal ore deposits, which have a narrow range of $\delta^{65}Cu$ values mainly between – 1 and +1‰ (Mathur et al., 2009) (Fig. 5). The granitoids in the Yenice region are magnesian, calc-

alkalic, and metaluminous, with an I-type character (Çiçek et al., 2017b). At hydrothermal-magmatic temperatures (>300ºC), Cu isotope fractionation between sulfides and fluids is negligible (Larson et al., 2003; Graham et al., 2004). Indeed, the δ^{65}Cu value obtained from the Soğucak porphyry (+0.13‰) was obtained from the inner pyropylitic alteration zone, and is similar to the average δ^{65}Cu value of I-type granites in the upper continental crust is +0.03 ± 0.15‰ (Li et al., 2009). This alteration zone forms as prograde and transitional alteration zone in Soğucak where may pass downwards to potassic alteration at the deeper parts of the porphyry (Corbett, 2017). The δ^{65}Cu value in the Soğucak phyllic alteration zone (+0.77‰) is significantly higher than in the core of the deposit. Phyllic alteration zone may result in the replacement of mafic minerals (i.e., hornblende, pyroxene, and biotite) by quartz-sericite-pyrite in acidic conditions as a retrograde hydrothermal alteration in the process of magmatic and meteoric fluid mixing (Giggenbach, 1997; Corbett, 2017) or subsequent cooling of the magmatic fluids (Hedenquist et al., 1998; Harris and Golding, 2002). The lower value mainly characterizes the high-temperature inner pyropylitic/potassic alteration at depth, whereas higher values correspond to phyllic alteration. This observation is in accord withobservations from similar deposits worldwide, which also show an increase in δ^{65}Cu values from sulfides in the potassic core zones to the more distal phyllic and advanced argillic alteration zones (Li et al., 2010; Mathur et al., 2013; Duan et al., 2016; Gregory and Mathur, 2017). These variations in Cu isotope signatures are attributed to changes in pH conditions (near neutral to acidic) and Cu speciation ($CuHS^0$ to $CuCl_2^-$) at different stages of magmatic-hydrothermal evolution (Mathur et al., 2013; Gregory and Mathur, 2017). Similarly, the skarn mineralization at Soğucak lies at the contact between carbonate rocks and intrusion, which is also a later alteration stage formed in cooler regions of the porphyry-skarn environment (+0.52‰).

Samples from the Arapuçandere Pb-Zn-Cu (Ag-Au) epithermal deposit have δ^{65}Cu values that range from – 0.05 to +0.46‰ (Fig. 5). Overall, the data from this deposit are similar

to the δ^{65}Cu values observed within the high-sulfidation Zijinshan epithermal Cu-Au deposit (South China), which shows a narrow range in δ^{65}Cu values in primary (hypogene) minerals (predominantly from – 0.49 to +0.39‰) that decrease with increasing depth (Wu et al., 2017). There is no consistent trend in δ^{65}Cu values with depth in the Arapuçandere deposit, but fluid inclusion studies and geochemical analyses indicate that two of the samples (+0.46‰; sample 160-V5-2 and + 0.35‰; sample 200-V4-4) were taken from the boiling zone (Çiçek et al., 2017b). During phase separation, ^{65}Cu is preferentially partitioned into the vapor phase (Yao et al., 2016), hence it is possible that these two samples were influenced by this process. The surface samples from across the Yenice region show a narrow range in δ^{65}Cu values from – 0.07 to +0.18‰ (– 0.07‰, Kozcağız-I Pb-Zn-Cu vein; +0.12‰, Sofular intraplutonic Cu veinlets; +0.16‰, Alandere distal skarn; +0.18‰; Arapuçandere surface). By comparison, Mirnejad et al. (2010) and Duan et al. (2016) found wide ranges of – 6.16 to +4.82‰ and – 4.76 to +2.84‰ in similar porphyry and high-sulfidation Cu deposits from Iran and Tibet, respectively. Mirnejad et al. (2010) demonstrated Cu isotopic trends in oxide and sulfide minerals from leached cap (i.e., hematite, goethite, jarosite, malachite), supergene (i.e., chalcocite, pyrite, hematite) and hypogene (i.e., pyrite, chalcopyrite) zones in the porphyry Cu deposits from the Kerman belt of Iran and noticed that the lightest values are from the leached cap and the heaviest values were found in supergene minerals. Similarly, Duan et al. (2016) reported the copper isotopic compositions in sulfide minerals (i.e., digenite, bornite, tetrahedrite, enargite, and covellite) from the Tiegelongnan high-sulfidation copper deposit (Tibet) and defined a systematic increase in the copper isotopic values with depth. This study (Duan et al., 2016) pointed out that the wide Cu isotopic variation of up to +7.8‰ reflects low-temperature supergene processes which indicate a significant isotope fractionation during low-temperature leaching of sulfides under oxidizing conditions. Hence, another possibility is that

isotopically heavier chalcopyrite values in the Yenice region may be indicating a supergene process of the chalcopyrite in Cu mineralization.

The results of the copper isotope study of Soğucak-Arapuçandere magmatic-hydrothermal systems show that the physicochemical properties of the hydrothermal fluids evolved during the mineralization process led to isotopic fractionation of the sulfides. As a general trend, chalcopyrite and pyrite crystallized in the early stage of mineralization have a narrow range of copper isotope values close to 0‰, and as the fluid moves away from the source and the temperature drops, sulfides possess heavier copper isotope values, creating a vector from the proximal to distal portions of the magmatic-hydrothermal environment in the Yenice region. In this setting, the data suggest that the change in the Cu isotope signature of sulfide (pyrite-chalcopyrite) resulted in the Cu isotope fractionation between the magmatic fluid and precipitating sulfides due to variations in pH and progressive cooling of magmatic-hydrothermal fluids along the fluid pathway.

7.1.2. Fe isotopic zonation

The δ^{56}Fe values of pyrite and chalcopyrite range from – 1.06 to +0.46‰ (Table 2). Pyrites from the skarn and porphyry alteration zones at Soğucak yield relatively heavier δ^{56}Fe values (+0.17 to +0.46‰) than those from Arapuçandere and other sites in the Yenice region, all of which have δ^{56}Fe < 0‰.

The pyrite formed during the early stage of the Soğucak skarn, has a δ^{56}Fe value of +0.17‰ (sample SS-3), within the range of δ^{56}Fe values (– 0.08 to +0.21‰) observed in I-type granites (Fig. 6) (Foden et al., 2015). In comparison, the two disseminated pyrites from the Soğucak alteration zone have similar δ^{56}Fe values of +0.44‰ (inner pyropylitic zone; SP-2) and +0.46‰ (phyllic zone; SP-5). This observation suggests that as the ore forming fluid exsolved from the cooling magma chamber it evolved towards heavier Fe isotope ratios. One possible explanation is that the pyrite formed after crystallization of Fe-Mg silicates in the

intrusion because light Fe isotopes are preferentially incorporated into Fe-bearing silicates during fractionation (Wawryk and Foden, 2017). The high δ^{56}Fe values in the disseminated pyrites are also similar to the pyrite Fe isotopic compositions reported from three other porphyry deposits elsewhere (Li et al., 2018; Zhu et al., 2018; He et al., 2020).

The 7 pyrite samples from the veins within the Arapuçandere deposit have δ^{56}Fe values that range from – 0.73 to – 0.43‰, all of which are lighter than the range observed in I-type granites. There are various competing factors operating during the crystallization of magnetite and sulfides in mineralized systems, which act to drive the δ^{56}Fe values of minerals and fluids to both higher and lower values. In general, however, high-silica igneous rocks (>70 wt% SiO_2) have higher δ^{56}Fe values than mafic to intermediate composition igneous rocks (<70 wt% SiO_2) (Heimann et al., 2008). The crystallization of Fe(II)-bearing silicate minerals drives the residual magma and/or fluid to heavier δ^{56}Fe values, whereas crystallization of high-Fe^{3+} magnetite leads to the relative enrichment of the hydrothermal ore-forming fluid in light Fe (Bullen et al., 2001; Johnson et al., 2002; Anbar et al., 2005). Similarly, the incorporation of heavy iron isotopes during the crystallization of pyrite and magnetite in the Soğucak porphyry and skarn zone leads to the enrichment of light iron isotopes in the residual magmatic-hydrothermal fluid. At Arapuçandere deposit, the δ^{56}Fe values return to lighter initial isotopic values (– 0.73‰) with the onset of a new cycle of iron isotopic fractionation. Theoretical studies show that both pyrite and chalcopyrite are also enriched in heavy Fe isotopes relative to hydrothermal fluids in equilibrium reactions (Polyakov et al., 2007; Polyakov and Soultanov, 2011). However, kinetic effects can lead to pyrite forming with δ^{56}Fe values that are lighter than hydrothermal fluids (Butler et al., 2005; Guilbaud et al., 2011) and the potential lack of isotopic equilibria between both mineral pairs and mineral-fluids in hydrothermal systems (Zhu et al., 2016; He et al., 2020) is a further complicating factor. In the absence of kinetic and non-equilibrium effects, the light δ^{56}Fe values in the Arapuçandere pyrite may thus reflect fluids

derived from a high-silica igneous source, or formation from fluids that have previously been depleted in heavy Fe isotopes through crystallization of a ^{56}Fe-enriched phase.

An alternative hypothesis is that the magmatic-hydrothermal fluids interacted with host rocks containing light Fe isotope compositions. For example, the shift of chalcopyrite and pyrite to lighter δ^{56}Fe values in the skarn mineralization of the Grasberg igneous complex has been hypothesized to be due to the assimilation of Fe from sedimentary rocks (Graham et al., 2004).

7.2. Sulfur isotope composition and its source

The δ^{34}S values of sulfides from the various types of mineralization in the Yenice region, combined with results from previous studies, yield a range of – 4.0 to 3.9‰ (Fig. 7; Table 3), which are in the range of δ^{34}S values of sulfides from epithermal deposits in Biga Peninsula. Collectively, the δ^{34}S values of sulfides decrease in the order pyrite > sphalerite > chalcopyrite > galena (Fig. 7), indicating equilibrium sulfur isotope fractionation between sulfides (Sakai, 1968; Bachinski, 1969). The pyrite and chalcopyrite samples from Soğucak porphyry alteration and skarn, and Sofular intraplutonic Cu veinlets show enrichment in δ^{34}S and are more positive than the δ^{34}S values of sulfides from the other mineralization at Yenice region. Granitoid rocks show a wide range of δ^{34}S values between – 11 and 14.5‰ with an average of 1.0 ± 6.1‰ (Seal, 2006), whereas ore-forming fluids with significant heterogeneous and lower δ^{34}S values of less than – 15‰ are typical to that of sedimentary origin (Goldfarb et al., 1991; Wilson et al., 2007). In addition, Sasaki and Ishihara (1979) and Ishihara and Sasaki (1989) found the discernible difference between δ^{34}S in the magnetite-series and ilmenite-series granitoids. δ^{34}S values >0‰ correspond to sulfur from magnetite-series granitoids (I-type) which is mostly clustering around 5‰, whereas δ^{34}S values <0‰ characterizes ilmenite-series granitoids (S-type). Considering that the Soğucak, Sofular, and other plutons in the Yenice region are of I-type and magnetite-series granitoids (e.g., Aysal, 2015; Çiçek et al.,

2017b; Aydın et al., 2019), it is more likely that positive $\delta^{34}S$ values imply a magmatic source of sulfur for crystallized pyrite and chalcopyrite from mineralization and alteration.

The sulfides (i.e., sphalerite, galena, and chalcopyrite) from the II-IV-V veins within the Arapuçandere deposit have $\delta^{34}S$ values that range from – 4.0 to 0.6‰, the vast majority of which are negative and lower than the range observed in Soğucak and Sofular. A compilation of the $\delta^{34}S$ values is shown for various epithermal deposits in Biga Peninsula in Fig. 7 and demonstrates that these deposits reveal S isotope variations within the range in the granitoid rocks worldwide (Oyman, 2019). Previously published sulfur isotope data currently exists on only Arapuçandere deposit in the Yenice region. Orgün et al. (2005) provided the first sulfur isotope data from pyrite and galena at Arapuçandere and point out that the sulfur and metals mainly originated from an igneous source. More detailed studies (including O, H, S, and Pb isotopes, and crushed leach studies of fluid inclusions) also indicate that sulfur was derived from Cenozoic magmatism, with the fluids showing mixing between meteoric water and magmatic fluid, and the precipitation of the ore metals resulting from boiling of the ore-forming fluids at the time of mineralization (Bozkaya et al., 2008; Bozkaya, 2011; Bozkaya and Banks, 2015). Similarly, data presented here show that the Arapuçandere deposit displays fairly homogeneous $\delta^{34}S$ values close to 0‰, hence a potential involvement of sedimentary sulfur from basement rocks is unlikely during the formation of the veins. To constrain more precisely the source of sulfur at the Yenice region, the sulfur isotope systematics for sulfides from the other mineralization was investigated, which have mostly negative $\delta^{34}S$ values, and are similar to the $\delta^{34}S$ values of sulfides from the Arapuçandere deposit.

In addition, ore petrography observations show that galena and sphalerite were formed contemporaneously in similar conditions in the ore deposition stage of the Arapuçandere deposit. Assuming equilibrium conditions between coexisting mineral pairs (Seal, 2006), sulfur isotope geothermometry has been applied to sphalerite-galena pairs from the Arapuçandere

deposit. Three mineral pairs display a narrow range of equilibrium temperatures from 292.3 to 297.8°C, which are consistent with the measured homogenization temperatures from the fluid inclusions by the previous studies (Orgün et al., 2005; Bozkaya et al., 2008; Bozkaya and Banks, 2015; Çiçek et al., 2017).

$\delta^{34}S_{sulfate}$-$\delta^{34}S_{sulfide}$ diagrams can be used to estimate the ratio of oxidized to reduced S species (SO_4^{2-}/H_2S) and the total S isotope values($\delta^{34}S_{\Sigma S}$) of the fluid source (e.g., Fifarek and Rye, 2005; Seal, 2006; Hutchison et al., 2020). Although there are no isotopic values of sulfates in the Yenice region, these plots can be drawn based on $\delta^{34}S$ values of sulfides and temperatures estimated by other techniques such as fluid inclusions (Li et al., 2016). We used the average homogenization temperatures of fluid inclusions to estimate temperatures based on previous studies of Çiçek et al. (2017a), Çiçek et al. (2017b) and Çiçek and Oyman (2019a), Çiçek and Oyman (2019b), and calculated the $\delta^{34}S$ values of H_2S_{aq} in equilibrium with the sulfides using the equation of Ohmoto and Rye (1979). Exceptionally, the $\delta^{34}S$-H_2S_{aq} values of sulfides in the Alandere Pb-Zn-Cu distal skarn were calculated by using the highest (450°C) and lowest (250°C) temperatures obtained from mineral chemistry geothermometry of the sulfarsenides. The overall $\delta^{34}S$ values of H_2S_{aq} in equilibrium with the sulfides from the Yenice region (Table 3, Fig. 8) is between – 2.1 to 2.7‰ that falls in the lines between the H_2S dominated reduced ($SO_4^{2-}/H_2S = 0$) and equal proportions of SO_4^{2-} and H_2S ($SO_4^{2-}/H_2S = 1$) systems. A chalcopyrite sample from the Sofular intraplutonic Cu veinlets, two pyrite samples from the Soğucak Fe ± Cu skarn plot into the porphyry field, whereas sulfides (i.e., galena, sphalerite and chalcopyrite) from the Alandere Pb-Zn-Cu distal skarn plot into both porphyry and high sulfidation epithermal fields in Fig. 8. In contrast, $\delta^{34}S$ values of H_2S_{aq} in equilibrium with sulfides from the Arapuçandere, Kozcağız-I, Tepetarla mineralization, together with pyrite from inner propylitic alteration at Soğucak, all fall within the high sulfidation epithermal field and follow the horizontal H_2S-dominated line towards transition/intermediate and low

sulfidation systems (Fig. 8), suggesting the ore-forming fluids probably were dominated by H_2S under relatively reducing conditions. Hydrothermal systems associated with I-type granitoids mostly show more sulfur isotopic variations due to subequal proportions of SO_2 and H_2S in the fluids (Seal, 2006). Hence, these observations likely reflect the ore-forming mechanism between mineralization and local magmatism that could be generated through progressive cooling and transition in a redox state (i.e., SO_4^{2-} /H_2S) of the hydrothermal fluids at the time of mineralization (Giggenbach, 1997; Hutchison et al., 2020).

7.3. Lead isotope composition and its source

All the mineralization sites in the Yenice region show a limited variation in Pb isotope ratios and they all fall within the ranges recorded from the Arapuçandere deposit, except for the Alandere distal skarn sample (Table 4). The data are compared to the Pb isotope compositions of magmatic rocks in the region in Fig. 9, together with previously published data for galena and pyrite from the Arapuçandere, Koru, Tesbihdere, Çataltepe and Kalkım deposits (Fig. 1). All the data fall within the fields defined by Aegean to West Anatolian Oligocene-Miocene Magmatic rocks (AOMM) (Ersoy and Palmer, 2013 and references therein), with the exception of the Soğucak porphyry samples that are slightly more radiogenic and lie within the range for granitoid rocks in the Yenice region. On the $^{206}Pb/^{204}Pb$ – $^{207}Pb/^{204}Pb$ and $^{206}Pb/^{204}Pb$ – $^{208}Pb/^{204}Pb$ diagrams (Fig. 9A and C), all the ore mineral data plot above the upper crust evolution curve (Zartman and Doe, 1981).

The Pb isotope data from mineralization in the Yenice region and from the Kalkım deposit plot in a restricted area than obtained by Bozkaya (2011). They also form data fields that are distinct from data from the Koru, Tesbihdere and Çataltepe deposits (Fig. 9B and D), although it is important to note that all the data from the Biga Peninsula lie within the fields defined by magmatic rocks from the region. The slightly higher $^{206}Pb/^{204}Pb$, and lower $^{207}Pb/^{204}Pb$ and $^{208}Pb/^{204}Pb$ isotope ratios than those of Yenice and Kalkım indicate that most

of their Pb is derived from the Oligocene-Miocene magmatic rocks, but possibly with smaller contributions from the Eocene magmatic rocks (Bozkaya and Gökçe, 2009; Çiçek and Oyman, 2016).

This interpretation contrasts with that of Bozkaya (2011), who calculated the Pb-isotope model ages of the Arapuçandere deposit to range from 114 to 63 Ma (Early Cretaceous to Palaeocene), and suggested that the Pb was derived from the Triassic rocks of the Karakaya Complex. It was further suggested that there is no genetic relationship between mineralization and the Oligocene granitoids, and that emplacement of the granitoids occurred after ore formation in Arapuçandere. In contrast, Akiska et al. (2013) concluded that Pb in galena from the Kalkım Pb-Zn ± Cu distal skarn deposits in the southeast of the Biga Peninsula was derived from local magmatic activity, albeit with a small contribution from the host rock (graphite schists). Overall, the Pb isotope data presented here suggest that the Pb mineralization in the Yenice Region was almost exclusively derived from local magmatic sources, and any contribution of Pb from the basement rocks, such as the Nilüfer and Hodul units of the Karakaya Complex, was relatively minor.

8. Conclusions

Variation of Cu, Fe, S and Pb isotope in sulfides from the various types of mineralization from the Yenice region provide important insights into metal source and ore-forming fluid evolution in the area. The $\delta^{56}Fe$ and $\delta^{65}Cu$ values in the Yenice region range from – 1.06 to +0.46‰ and – 0.07 to +0.77‰, respectively. All the regional plutons have an I-type character, which typically have $\delta^{56}Fe$ values that range from – 0.08 to 0.21‰, and $\delta^{65}Cu$ values of +0.03 ± 0.15‰, worldwide. The heaviest $\delta^{56}Fe$ values (+0.44 and +0.46‰) were measured in pyrites from the Soğucak porphyry alteration zone, pyrite samples from veins within the epithermal Arapuçandere deposit have light $\delta^{56}Fe$ values of – 0.73 to – 0.43‰. In the absence

of Fe assimilation from the basement rocks, these ranges likely reflect the complex interplay of redox, Rayleigh and kinetic effects.

None of the $\delta^{65}Cu$ values extend to the heavy values (~+6‰) observed in supergene and light values (~-5‰) observed in leached cap minerals in ore deposits from elsewhere in the world. Rather, the data lie in the – 1 to +1‰ range in typical primary (hypogene) minerals in magmatic-hydrothermal ore deposits. The $\delta^{65}Cu$ value in the phyllic alteration zone Soğucak skarn mineralization is significantly higher (+0.77‰) than in the core of the deposit (+0.13‰); in accord with observations from similar deposits worldwide. The Cu isotope values of chalcopyrite from the Arapuçandere deposit tend to progressively increase through the surface, which creates a vector from the proximal to distal portions of the magmatic-hydrothermal environment, possibly with local supergene processes within the deposit.

The $\delta^{34}S$ values of sulfides from the mineralization in the Yenice region exhibit a relatively narrow range in $\delta^{34}S$ (– 4.0 to 3.9‰), consistent with the magmatic origin for sulfur. All data lie within the range of $\delta^{34}S$ values reported from various epithermal deposits (high to low sulfidation) in the Biga Peninsula. The calculated $\delta^{34}S$ values of H_2S_{aq} in equilibrium with the sulfides that plot into the porphyry and high sulfidation fields indicate an ore-forming mechanism related to progressive cooling and transition of the hydrothermal fluids that were dominated by H_2S under relatively reducing conditions. Moreover, the sulfide samples have relatively homogeneous Pb isotope compositions $^{206}Pb/^{204}Pb$, $^{207}Pb/^{204}Pb$, and $^{208}Pb/^{204}Pb$ values, indicative of a common source of lead for the mineralization in the Yenice region. All the Pb isotope data (including the whole rocks) fall within a narrow range that lies wholly within the field defined by the Oligocene to Miocene magmatic rocks in the Biga Peninsula. These observations support the hypothesis that the metals and sulfur contained within all the various styles of deposits considered here were derived entirely from these magmatic rocks, with no significant contamination from the local basement rocks.

In summary, calc-alkaline and I-type magmatism gave rise to the formation of an important magmatic-hydrothermal environment in the Yenice region between the Late Oligocene and the Early Miocene. The ore-forming fluids responsible for mineralization are generated through progressive cooling and transition in a redox state (i.e., SO_4^{2-} /H_2S) and resulted in the formation of the Soğucak porphyry-skarn mineralization and associated Arapuçandere intermediate sulfidation epithermal deposit. The physicochemical properties of the fluids that evolved during the metal deposition led to Cu and Fe isotopic fractionation of the sulfides (i.e., pyrite and chalcopyrite) in the Soğucak-Arapuçandere magmatic-hydrothermal system (Fig. 10). At Soğucak, the δ^{65}Cu lower value mainly characterizes the high-temperature inner pyropylitic/potassic alteration at depth, whereas higher values correspond to phyllic alteration and skarn zone. Conversely, isotopically heavier Fe isotope signatures indicate the incorporation of heavy iron isotopes during the crystallization of pyrite and magnetite in the Soğucak porphyry and skarn zone which leads to the enrichment of light iron isotopes in the residual magmatic-hydrothermal fluid. In the hydrothermal phase, Arapuçandere deposit associated with porphyry intrusion appears to reflect the isotopic fractionation of Cu and Fe that occurred in the vein bodies during fluid exsolution from the residual magmatic-hydrothermal fluid due to physicochemical conditions, and Rayleigh type fractionation processes between the fluid and chalcopyrite-pyrite crystallizations. The pyrite and chalcopyrite in both veins broadly show an increase in iron and copper isotope values from the deeper levels of early stage mineralization to the more distal/upper levels of late stage mineralization, with the exception of the two samples (i.e., 160-V5-2 and 200-V4-4) that were possibly influenced by boiling effects.

Declaration of Competing Interest

The authors declare that they have no known competing financial interests or personal relationships that could have appeared to influence the work reported in this paper.

Acknowledgments

This study is a part of the Ph.D. thesis of the first author at the Geological Department of Dokuz Eylül University supervised by Dr. Tolga Oyman. Financial support of this study was provided by the Scientific and Technological Research Council of Turkey (TÜBİTAK) via a research project (ÇAYDAG - 114Y055). We thank Dr. Ryan Mathur and second anonymous reviewer for their constructive revisions and comments on earlier versions of this manuscript. We also thank Dr. Franco M. Pirajno for the editorial handling. We are most grateful to the Esan and Nesco Mining Company for the close cooperation and unlimited access to collect the surface and drill core samples from the Soğucak porphyry and underground samples from the Arapuçandere deposit.

References

Ağdemir, N., Kırıko˘glu, M.S., Lehmann, B., Tietze, J., 1994. Petrology and alteration geochemistry of the epithermal Balya Pb-Zn-Ag deposit. NW Turkey. Mineral. Deposita 29, 366–371.

Akal, C., 2013. Coeval shoshonitic-ultrapotassic dyke emplacements within the Kestanbol pluton, Ezine - Biga Peninsula (NW Anatolia). Turk. J. Earth Sci. 22, 220–238.

Akbas¸, B., Akdeniz, N., Aksay, A., Altun, I., Balcı, V., Bilginer, E., Bilgiç, T., Duru, M., Ercan, T., Gedik, I., Günay, Y., Güven, I.H., Hakyemez, H.Y., Konak, N., Papak, I., Pehlivan, S¸., Sevin, M., Şenel, M., Tarhan, N., Turhan, N., Türkecan, A., Ulu, Ü., Uğuz, M.F., Yurtsever, A., 2017. Geological map of Turkey. General Directorate of Mineral Research and Exploration Publication, Ankara-Turkey.

Akıska, S., Demirela, G., Sayılı, S.I., 2013. Geology, mineralogy and the Pb, S isotope study of the Kalkım Pb-Zn ± Cu deposits, Biga Peninsula, NW Turkey. J. Geosci. 58, 379–396.

Aldanmaz, E., Pearce, J.P., Thirlwall, M.F., Mitchell, J.G., 2000. Petrogenetic evolution of late Cenozoic, post-collision volcanism in western Anatolia. Turkey. J. Volcanol. Geotherm. Res. 102, 67–95.

Altunkaynak, S., Dilek, Y., 2013. Eocene mafic volcanism in northern Anatolia: its causes and mantle sources in the absence of active subduction. Int. Geol. Rev. 55, 1641–1659.

Altunkaynak, Ş., Sunal, G., Aldanmaz, E., Genç, C.Ş., Dilek, Y., Furnes, H., Foland, K.E., Yang, J., Yıldız, M., 2012a. Eocene granitic magmatism in NW Anatolia (Turkey) revisited: new implications from comparative zircon SHRIMP U-Pb and ^{40}Ar-^{39}Ar geochronology and isotope geochemistry on magma genesis and emplacement. Lithos 155, 289–309.

Altunkaynak, Ş., Dilek, Y., Genç, C. Ş., Sunal, G., Gertisser, R., Furnes, H., Foland, K.A., Yang, J., 2012b. Spatial, temporal and geochemical evolution of Oligo-Miocene granitoid magmatism in western Anatolia. Turkey. Gondwana Res. 21, 961–986.

Altunkaynak, Ş., Genç, C. Ş., 2008. Petrogenesis and time-progressive evolution of the Cenozoic continental volcanism in the Biga Peninsula, NW Anatolia (Turkey). Lithos 102, 316–340.

Anbar, A.D., Jarzecki, A.A., Spiro, T.G., 2005. Theoretical investigation of iron isotope fractionation between $Fe(H_2O)_6^{3+}$ and $Fe(H_2O)_6^{2+}$: Implications for iron stable isotope geochemistry. Geochim. Cosmochim. Acta 69, 825–837.

Anıl, M., 1979. Etude geologique et metallogenique du secteur septrional de Yenice (Presqu'ile de Biga-Turquie). PhD Thesis, Ecole de Geologie, Université de Nancy, France, 142 pp. (Unpublished).

Anıl, M., 1984. Genesis of the Pb-Zn-Cu mineralization and relations with Tertiary volcanism in Yenice area (Arapuçandere-Kurttas¸ı, Sofular and Kalkım-Handeresi). J. Geol. Eng. 20, 17–30 (in Turkish with English abstract).

Anıl, M., Yaman, S., 1985. Fluid inclusions studies on the Arapuçandere (Yenice-Çanakkale) Pb-Zn mineralizations. Bull. Earth Sci. Application and Research Centre Hacettepe Univ. 12, 81–91.

Atılgan, I., 1977. The geological survey of the north of Arapuçandere-Kurttas¸ı and Yenice. Mineral Research and Exploration Institute of Turkey (MTA), unpublished report (in Turkish).

Aydın, Ü., Şen, P., Özmen, Ö., Şen, E., 2019. Petrological and geochemical features of Biga Peninsula granitoids, NW Anatolia, Turkey. Bulletin of the Mineral Research and Exploration 160, 81–115. Ş

Aysal, N., 2015. Mineral chemistry, crystallization conditions and geodynamic implications of the Oligo-Miocene granitoids in the Biga Peninsula. Northwest Turkey. J. Asian Earth Sci. 105, 68–84.

Bachinski, D.J., 1969. Bond strength and sulfur isotopic fractionation in coexisting sulfides. Econ. Geol. 64, 56–65.

Baxter, D.C., Rodushkin, I., Engström, E., Malinovsky, D., 2006. Revised exponential model for mass bias correction using an internal standard for isotope abundance ratio measurements by multi-collector inductively coupled plasma-mass spectrometry. J. Anal. Atom. Spectrom. 21, 427–430.

Beccaletto, L., Bartolini, A.C., Martini, R., Hochuli, P.A., Kozur, H., 2005. Biostratigraphic data from the Çetmi mélange, northwest Turkey. Palaeogeographic and tectonic implications. Palaeogeogr. Palaeoclimatol. Palaeoecol. 221, 215–244.

Borrok, D.M., Nimick, D.A., Wanty, R.B., Ridley, W.I., 2008. Isotopic variations of dissolved copper and zinc in stream waters affected by historical mining. Geochim. Cosmochim. Acta 72, 329–344.

Bozkaya, G., 2011. Sulphur- and lead-isotope geochemistry of the Arapuçandere lead-zinc-copper deposit, Biga Peninsula, Northwest Turkey. Int. Geol. Rev. 53, 116–129.

Bozkaya, G., Banks, A.D., 2015. Physico-chemical controls on ore deposition in the Arapucandere Pb-Zn-Cu-precious metal deposit, Biga Peninsula. NW Turkey. Ore Geol. Rev. 66, 65–81.

Bozkaya, G., Banks, D.A., Ozbas, F., Wallington, J., 2014. Fluid processes in the Tesbihdere base-metal-Au deposit: implications for epithermal mineralization in the Biga Peninsula. Central Eur. J. Geosci. 6, 148–169.

Bozkaya, G., Bozkaya, Ö., Banks, D.A., Gökçe, A., 2020. P-T-X constraints on the Koru epithermal base-metal (±Au) deposit, Biga Peninsula. NW Turkey. Ore Geol. Rev. 119, 103349.

Bozkaya, G., Gökçe, A., 2009. Lead and sulfur isotope studies of the Koru (Çanakkale, Turkey) lead-zinc deposits. Turk. J. Earth Sci. 18, 127–137.

Bozkaya, G., Gökçe, A., Grassineau, N.V., 2008. Fluid Inclusion and Stable Isotope Characteristics of the Arapuçandere Pb-Zn-Cu Deposits. Northwest Turkey. Int. Geol. Rev. 50 (9), 848–862.

Bozkurt, E., 2001. Neotectonics of Turkey-a synthesis. Geodinamica Acta 14, 3–30.

Braxton, D., Mathur, R., 2011. Exploration applications of copper isotopes in the supergene environment: A case study of the Bayugo porphyry copper-gold deposit, southern Philippines. Econ. Geol. 106, 1447–1463.

Bullen, T.D., White, A.F., Childs, C.W., Vivit, D.V., Schultz, M.S., 2001. Demonstration of significant abiotic iron isotope fractionation in nature. Geology 29, 699–702.

Butler, I.B., Archer, C., Vance, D., Oldroyd, A., Rickard, D., 2005. Fe isotope fractionation on FeS formation in ambient aqueous solution. Earth Planet. Sci. Lett. 236, 430–442.

Cavazza, W., Okay, A.I., Zattin, M., 2009. Rapid early-middle Miocene exhumation of the Kazdaˇg Massif (western Anatolia). Int. J. Earth Sci. 98, 1935–1947.

Chaussidon, M., Albaréde, F., Sheppard, S.M.F., 1989. Sulphur isotope variations in the mantle from ion microprobe analyses of micro-sulphide inclusions. Earth Planet. Sci. Lett. 92, 144–156.

Chakrabarti, R., Basu, A.R., Ghatak, A., 2012. Chemical geodynamics of Western Anatolia. Int. Geol. Rev. 54, 227–248.

Corbett, G.J., 2017. Epithermal Au-Ag and porphyry Cu-Au exploration-short course manual. Unpublished, Sept. 2017 edition.

Çağatay, A., 1980. Geology and mineralogy of western Anatolian lead-zinc deposits and some comments about their genesis. Bull. Geol. Soc. Turk. 23, 119–132.

Çiçek, M., Oyman, T., 2016. Origin and evolution of hydrothermal fluids in epithermal Pb-Zn-Cu ± Au ± Ag deposits at Koru and Tesbihdere mining districts, Çanakkale, Biga Peninsula. NW Turkey. Ore Geol. Rev. 78, 176–195.

Çiçek, M., Oyman, T., 2019a. Mineralogical and Geochemical characterization of Soğucak (Yenice, Çanakkale) Fe (±Cu) Skarn, Biga Peninsula, NW Turkey. 72nd Geological Congress of Turkey with international participation.

Çiçek, M., Oyman, T., 2019b. Copper and Iron Isotope Geochemistry of the Mineralization in the NE of Yenice (Çanakkale-Biga Peninsula), NW Turkey. In: International Earth Science Colloquium on the Aegean Region, p. 129.

Çiçek, M., Oyman, T., Kaliwoda, M., Hochleitner, R., 2017. Mineralogy and mineral chemistry of the Arapuçandere Pb-Zn-Cu (Ag-Au) mineralization in the northeast of Yenice (Çanakkale),

Biga Peninsula, NW Turkey. Workshop on Subduction Related Ore Deposits, Karadeniz Technical University, Trabzon-Turkey, Abs, Book, p. 18.

Çiçek, M., Oyman, T., Ozgenc, I., Akbulut, M., 2012. Fluid evolution of the Koru Pb-Zn deposit, Çanakkale (NW-Turkey). In: International Earth Science Colloquium on the Aegean Region, p. 158.

Çiçek, M., Oyman, T., Palmer, M.R., Catlos, E.J., Selby, D., Michalik, A., Cooper, M.J., 2017b. Geochronology and isotope (Sr, Nd and Pb) geochemistry of the Oligocene intrusions and associated hydrothermal mineralization in the northeast of Yenice, NW Turkey. Goldschmidt, 2017. Paris-France. Goldschmidt Abs, Book, p. 695.

Dayal, A., 1984. Yenice (Çanakkale) granitinin petrografisi ve buna baˇglı cevherles¸meler. Unpublished PhD Thesis, Dokuz Eylül Univ. The Graduate School of Natural and Applied Sciences, ˙Izmir (in Turkish).

Delaloye, M., Bingöl, E., 2000. Granitoids from western and northwestern Anatolia: geochemistry and modeling of geodynamic evolution. Int. Geol. Rev. 42, 241–268.

Demirela, 2011. Geology and genesis of the Çataltepe (Lapseki/Çanakkale) Pb- Zn±Cu±Ag deposit. Unpublished PhD Thesis, Ankara Univ. The Graduate School of Natural and Applied Sciences, Ankara (in Turkish with English abstract).

Dönmez, M., Akçay, A.E., Genç, Ş.C., Acar, Ş., 2005. Biga Yarımadasında Orta-Üst Eosen Volkanizması ve Denizel ˙Ignimbiritler. Bull. Mineral Res. Explor. Turk. 131, 49–61 (In Turkish).

Duan, J., Tang, J., Li, Y., Liu, S.A., Wang, Q., Yang, C., Wang, Y., 2016. Copper isotopic signature of the Tiegelongnan high-sulfidation copper deposit, Tibet: Implications for its origin and mineral exploration. Min. Dep. 51, 591–602.

Duru, M., Pehlivan, Ş., Şentürk, Y., Yavas¸, F., Kar, H., 2004. New results on the lithostratigraphy of the Kazdaˇg Massif in Northwest Turkey. Turk. J. Earth Sci. 13, 177–186.

Emre, Ö., Duman, T.Y., Özalp, S., Elmacı, H., Olgun, Ş., Şaroğlu, F., 2013. 1/1.125.000 scaled active faults map of Turkey. General Directorate of Mineral Research and Exploration, Sp. Publ. Series-30, Ankara-Turkey.

Ercan, T., Satır, M., Steinitz, G., Dora, A., Sarıfakıoğlu, E., Adis, C., Walter, H.-J., Yıldırım, T., 1995. Biga yarımadası ile Gokçeada, Bozcaada ve Tavs¸an adalarındaki (KB Anadolu) Tersiyer volkanizmasının ozellikleri. Bull. Mineral Res. Explor. Turk. 117, 55–86 (In Turkish).

Ercan, T., Türkecan, A., Guillou, H., Satır, M., Sevin, D., Şaroğlu, F., 1998. Marmara Denizi çevresindeki Tersiyer volkanizmasının ozellikleri. Bull. Mineral Res. Explor. Turk. 120, 199–221 (In Turkish).

Ersoy, E.Y., Akal, C., Genç, Ş.C., Candan, O., Palmer, M.R., Prelevic, D., Uysal, I., Mertz-Kraus, R., 2017. U-Pb zircon geochronology of the Paleogene - Neogene volcanism in the NW Anatolia: Its implications for the Late Mesozoic-Cenozoic geodynamic evolution of the Aegean. Tectonophysics 717, 284–301.

Ersoy, E.Y., Palmer, M.R., 2013. Eocene-Quaternary magmatic activity in the Aegean: implications for mantle metasomatism and magma genesis in an evolving orogeny. Lithos 180–181, 5–24.

Fifarek, R.H., Rye, R.O., 2005. Stable-isotope geochemistry of the Pierina high-sulfidation Au-Ag deposit, Peru: Influence of hydrodynamics on SO_4^{2-}–H_2S sulfur isotopic exchange in magmatic-steam and steam-heated environments. Chem. Geol. 215, 253–279.

Foden, J., Sossi, P.A., Wawryk, C.M., 2015. Fe isotopes and the contrasting petrogenesis of A-, I-and S-type granite. Lithos 212, 32–44.

Genç, Ş.C., D¨onmez, M., Akçay, A.E., Altunkaynak, Ş., Eyüpoğlu, M., Ilgar, Y., 2012. Biga Yarımadası Tersiyer volkanizmasının stratigrafik, petrografik ve kimyasal ozellikleri. In: Yüzer, E., Tunay, G. (Eds.), Biga Yarımadasının Genel ve Ekonomik Jeolojisi. Bulletin of the Mineral Research and Exploration, Special Publications 28. pp. 122- 162.

Georgiev, S., von Quadt, A., Heinrich, C.A., Peytcheva, I., Marchev, P., 2012. Time evolution of a rifted continental arc: integrated ID-TIMS and LA-ICPMS study of magmatic zircons from the Eastern Srednogorie, Bulgaria. Lithos 154, 53–67.

Giggenbach, W.F., 1997. The origin and evolution of fluids in magmatic-hydrothermal systems. In: Bames, H.L. (Ed.), Geochemistry 'of hydrothermal ore deposits. John Wiley and Sons, New York, pp. 737–796.

Goldfarb, R.J., Newberry, R.J., Pickthorn, W.J., Gent, C.A., 1991. Oxygen, hydrogen, and sulfur isotope studies in the Juneau gold belt, Southeastern Alaska - constraints on the origin of hydrothermal fluids. Econ. Geol. Bull. Soc. Econ. Geol. 86, 66–80.

Graham, S., Pearson, N., Jackson, S., Griffin, W., O'Reilly, S.Y., 2004. Tracing Cu and Fe from source to porphyry: in situ determination of Cu and Fe isotope ratios in sulfides from the Grasberg Cu-Au deposit. Chem. Geol. 207, 147–169.

Gregory, M.J., Mathur, R., 2017. Understanding copper isotope behavior in the high temperature magmatic-hydrothermal porphyry environment. Geochemistry, Geophysics, Geosystems 18, 4000–4015.

Guilbaud, R., Butler, I.B., Ellam, R.M., 2011. A biotic pyrite formation produces a large Fe isotope fractionation. Science 332, 1548–1551.

Gülmez, F., Genç, Ş.C., Keskin, M., Tüysüz, O., 2013. A post-collision slab-breakoff model for the origin of the Middle Eocene magmatic rocks of the Armutlu-Almacık belt, NW Turkey and its regional implications. In: Robertson, A.H.F., Parlak, O., Unlugenc, U. C. (Eds.), Geological Development of Anatolia and the Easternmost Mediterranean Region. Geol. Soc., London, Spec. Publ. 372, 107-139.

Gülmez, F., Genç, Ş.C., Prelevic, D., Tüysüz, O., Karacık, Z., Roden, M.F., Billor, Z., 2016. Ultrapotassic volcanism from the waning stage of the Neotethyan subduction: a key study from the Izmir-Ankara-Erzincan Suture Belt, Central Northern Turkey. J. Petrol. 57, 561–593.

Harris, A.C., Golding, S.D., 2002. New evidence of magmatic-fluid–related phyllic alteration: Implications for the genesis of porphyry Cu deposits. Geology 30, 335–338.

He, Z., Zhang, X., Deng, X., Hu, H., Li, Y., Yu, H., Archer, C., Li, J., Huang, F., 2020. The behavior of Fe and S isotopes in porphyry copper systems: Constraints from the Tongshankou Cu-Mo deposit. Eastern China. Geochim. Cosmochim. Acta 270, 61–83.

Hedenquist, J.W., Arribas, A., Reynolds, T.J., 1998. Evolution of an intrusion-centered hydrothermal system: Far Southeast-Lepanto porphyry and epithermal Cu-Au deposits, Philippines. Economic Geology 93, 373–404.

Heimann, A., Beard, B.L., Johnson, C.M., 2008. The role of volatile exsolution and sub-solidus fluid/rock interactions in producing high $^{56}Fe/^{54}Fe$ ratios in siliceous igneous rocks. Geochim. Cosmochim. Acta 72, 4379–4396.

Hoefs, J., 2009. Stable Isotope Geochemistry. Springer Verlag, Berlin, p. 285. Hutchison, W., Finch, A.A., Boyce, A.J., 2020. The sulfur isotope evolution of magmatic-hydrothermal fluids: insights into ore-forming processes. Geochim. Cosmochim. Acta 288, 176–198.

Ishihara, S., Sasaki, A., 1989. Sulfur isotopic ratios of the magnetite-series and ilmenite-series granitoids of the Sierra Nevada batholith - a reconnaissance study. Geology 17, 788–791.

Ishizuka, O., Taylor, R.N., Milton, A.J., Nesbitt, R., 2003. Fluid-mantle interaction in an intra-oceanic arc: constraints from high-precision Pb isotopes. Earth Planet. Sci. Lett. 211, 221–236.

Johnson, C.M., Skulan, J.L., Beard, B.L., Sun, H., Nealson, K.H., Braterman, P.S., 2002. Isotopic fractionation between Fe(III) and Fe(II) in aqueous solutions. Earth Planet Sci. Lett. 195, 141–153.

Karacık, Z., Yılmaz, Y., Pearce, J.A., Ece, Ö.I., 2008. Petrochemistry of the south Marmara granitoids, northwest Anatolia. Turkey. Int. J. Earth Sci. 97, 1181–1200.

Kidder, J.A., Voinot, A., Sullivan, K.V., Chipley, D., Valentino, M., Layton-Matthews, D., Leybourne, M., 2020. Improved ion-exchange column chromatography for Cu purification

from high-Na matrices and isotopic analysis by MC-ICPMS. J. Anal. At. Spectrom. 35, 776–783.

Krushensky, R.D., 1976. Neogene calc-alkaline extrusive and intrusive rocks of the Karalar-Yesiller area. Bull. Volcanol. 39, 336–360.

Kuşcu, I., Tosdal, R.M., Gençalioğlu-Kuşcu, G., 2019. Episodic porphyry Cu (-Mo-Au) formation and associated magmatic evolution in Turkish Tethyan collage. Ore. Geol. Rev. 107, 119–154.

Labidi, J., Cartigny, P., Birck, J.L., Assayag, N., Bourrand, J.J., 2012. Determination of multiple sulfur isotopes in glasses: A reappraisal of the MORB δ^{34}S. Chem. Geol. 334, 189–198.

Labidi, J., Cartigny, P., Jackson, M.G., 2015. Multiple sulfur isotope composition of oxidized Samoan melts and the implications of a sulfur isotope ‘‘mantle array” in chemical geodynamics. Earth Planet. Sci. Lett. 417, 28–39.

Labidi, J., Cartigny, P., Moreira, M., 2013. Non-chondritic sulphur isotope composition of the terrestrial mantle. Nature 501, 208–211.

Larson, P.B., Maher, K., Ramos, F.C., Chang, Z., Gaspar, M., Meinert, L.D., 2003. Copper isotope ratios in magmatic and hydrothermal ore-forming environments. Chem. Geol. 201, 337–350.

Li, J.X., Qin, K.Z., Li, G.M., Evans, N.J., Huang, F., Zhao, J.X., 2018. Iron isotope fractionation during magmatic-hydrothermal evolution: A case study from the Duolong porphyry Cu-Au deposit. Tibet. Geochim. Cosmochim. Acta 238, 1–15.

Li, J.X., Qin, K.Z., Li, G.M., Evans, N.J., Zhao, J.X., Cao, M.J., Huang, F., 2016. The Nadun Cu-Au mineralization, central Tibet: root of a high sulfidation epithermal deposit. Ore Geol. Rev. 78, 371–387.

Li, W., Jackson, S.E., Pearson, N.J., Alard, O., Chappell, B.W., 2009. The Cu isotopic signature of granites from the Lachlan Fold Belt, SE Australia. Chem. Geol. 258, 38–49.

Li, W., Jackson, S.E., Pearson, N.J., Graham, S., 2010. Copper isotopic zonation in the Northparkes porphyry Cu-Au deposit. SE Australia. Geochim. Cosmochim. Acta 74, 4078–4096.

Maher, K.C., Larson, P.B., 2007. Variation in copper isotope ratios and controls on fractionation in hypogene skarn mineralization at Coroccohuayco and Tintaya. Peru. Econ. Geol. 102, 225–237.

Marchev, P., Raicheva, R., Downes, H., Veselli, O., Chiaradia, M., Moritz, R., 2004. Compositional diversity of Eocene-Oligocene basaltic magmatism in the Eastern Rhodopes, SE Bulgaria: implications for genesis and tectonic setting. Tectonophys. 393, 301–328.

Maréchal, C., Télouk, P., Albaréde, F., 1999. Precise analysis of copper and zinc isotopic compositions by plasma-source mass spectrometry. Chem. Geol. 156, 251–273.

Markl, G., Wagner, T., Blanckenburg, F.V., 2006a. Iron isotope fractionation during hydrothermal ore deposition and alteration. Geochim. Cosmochim. Acta 70, 3011–3030.

Markl, G., Lahaye, Y., Schwinn, G., 2006b. Copper isotopes as monitors of redox processes in hydrothermal mineralization. Geochim. Cosmochim. Acta 70, 4215–4228.

Mathur, R., Jin, L., Prush, V., Paul, J., Ebersole, C., Fornadel, A., Brantley, S., 2012. Cu isotopes and concentrations during weathering of black shale of the Marcellus Formation, Huntingdon County, Pennsylvania (USA). Chemical Geology 304–305, 175–184.

Mathur, R., Munk, L., Nguyen, M., Gregory, M., Annell, H., Lang, J., 2013. Modern and paleofluid pathways revealed by Cu isotope compositions in surface waters and ores of the Pebble Porphyry Cu-Au-Mo Deposit. Alaska. Econ. Geol. 108, 529–541.

Mathur, R., Titley, S., Barra, F., Brantley, S., Wilson, M., Phillips, A., Hart, G., 2009. Exploration potential of Cu isotope fractionation in porphyry copper deposits. J. Geochem. Explor. 102, 1–6.

Mathur, R., Wang, D., 2019. Transition Metal Isotopes Applied to Exploration Geochemistry: Insights from Fe, Cu, and Zn. In: Decrèe S., Robb, L. (Eds.), Ore Deposits: Origin, Exploration, and Exploitation. Geophys. Monogr. Ser. Am. Geophys. Union 242, 163-184.

Menant, A., Jolivet, L., Tuduri, J., Loiselet, C., Bertrand, G., Guillou-Frottier, L., 2018. 3D subduction dynamics: A first-order parameter of the transition from copper- to gold-rich deposits in the eastern Mediterranean region. Ore Geol. Rev. 94, 118–135.

Mirnejad, H., Mathur, R., Einali, M., Dendas, M., Alirezaei, S., 2010. A comparative copper isotope study of porphyry copper deposits in Iran. Geochem: Explor. Env. Analysis 10, 413–418.

Moeller, K., Schoenberg, R., Pedersen, R.B., Weiss, D., Dong, S., 2012. Calibration of the New Certified Reference Materials ERM-AE633 and ERM-AE647 for Copper and IRMM-3702 for Zinc Isotope Amount Ratio Determinations. Geostandards and Geoanalytical Research 36, 177–199.

Moix, P., Beccaletto, L., Kozur, H.W., Hochard, C., Rosselet, F., Stampfli, G.M., 2008. A new classification of the Turkish terranes and sutures and its implication for the paleotectonic history of the region. Tectonophysics 451, 7–39.

MTA, 1993a. Gold and silver inventory of Turkey. MTA Publication 198, 1–46 (in Turkish).

MTA, 1993b. Lead-zinc inventory of Turkey. MTA Publication 199, 94 (in Turkish).

Ohmoto, H., Lasaga, A.C., 1982. Kinetics of reactions between aqueous sulfates and sulfides in hydrothermal systems. Geochim. Cosmochim. Acta 46, 1727–1745.

Ohmoto, H., Rye, R.O., 1979. Isotopes of sulfur and carbon. In: Barnes, H.L. (Ed.), Geochemistry of Hydrothermal Ore Deposits, second ed. Wiley, New York, pp. 509–567.

Okay, A.I., Göncüoğlu, M.C., 2004. The Karakaya Complex: a review of data and concepts. Turk. J. Earth Sci. 13, 77–95.

Okay, A.I., Satır, M., 2000. Coeval plutonism and metamorphism in a latest Oligocene metamorphic core complex in northwest Turkey. Geol. Mag. 138, 495–516.

Okay, A.I., Satır, M., Maluski, H., Siyako, M., Monie, P., Metzger, R., Akyüz, S., Yin, A., 1996. Paleo- and Neo-Tethyan events in northwestern Turkey: geologic and geochronologic constraints. In: Harrison, M. (Ed.), Tectonics of Asia. Cambridge University Press, pp. 420–441.

Okay, A.I., Siyako, M., Bürkan, K.A., 1991. Geology and tectonic evolution of the Biga peninsula, northwest Turkey. Bull. Istanbul Tech. Univ. 44, 191–256.

Okay, A.I., Tüysüz, O., 1999. Tethyan sutures of northern Turkey. In: Durand, B., Jolivet, L., Horváth, F., Séranne, M. (Eds.), The Mediterranean Basins: Tertiary extension within the Alpine orogen. Geological Society, London, Special Publication 156. pp. 475-515.

Orgün, Y., Gültekin, A.H., Önal, A., 2005. Geology, mineralogy and fluid inclusion data from the Arapuçandere Pb-Zn-Cu-Ag deposit, Çanakkale. Turkey. J. Asian Earth Sci. 25, 629–642.

Oyman, T., 2019. Epithermal Deposits of Turkey. In: Pirajno, F., Ünlü, C., Şahin, M., (Eds) Mineral Resources of Turkey. Modern Approaches in Solid Earth Sciences 16, Springer 159-223.

Öngen, S., 1982. Petrology of Yenice (Çanakkale) granitoids and host rocks. Associate Prof. Thesis, Istanbul University pp. 234 (in Turkish, unpublished).

Palacios, C., Rouxel, O., Reich, M., Cameron, E.M., Leybourne, M.I., 2011. Pleistocene recycling of copper at a porphyry system, Atacama Desert, Chile; Cu isotope evidence. Miner. Dep. 46, 1–7.

Polyakov, V.B., Clayton, R.N., Horita, J., Mineev, S.D., 2007. Equilibrium iron isotope fractionation minerals: Reevaluation from the data of nuclear inelastic resonant X-ray scattering and M¨ossbauer spectroscopy. Geochim. Cosmochim. Acta 71, 3833–3846.

Polyakov, V.B., Soultanov, D.M., 2011. New data on equilibrium iron isotope among sulfides: constraints on mechanisms of sulphide formation in hydrothermal and igneous systems. Geochim. Cosmochim. Acta 75, 1957–1974.

Picket, E.A., Robertson, A.H.F., 1996. Formation of the Late Paleozoic-Early Mesozoic Karakaya Complex and related ophiolites in NW Turkey by Paleotethyan subduction accretion. J. Geol. Soc. 153, 995–1009.

Richards, J.P., 2015. Tectonic, magmatic, and metallogenic evolution of the Tethyan orogen: From subduction to collision. Ore Geol. Rev. 70, 323–345.

Rye, R.O., 2005. A review of the stable-isotope geochemistry of sulfate minerals in selected igneous environments and related hydrothermal systems. Chem. Geol. 215, 5–36.

Sakai, H., 1968. Isotopic properties of sulfur compounds in hydrothermal processes. Geochem. J. 2, 29–49.

Sánchez, M.G., McClay, K.R., King, A.R., Wijbrams, J.R., 2016. Cenozoic crustal extension and its relationship to porphyry Cu-Au-(Mo) and epithermal Au-(Ag) mineralization in the Biga Peninsula, Northwest Turkey. Spec. Publ. - Soc. Econ. Geol. 19, 113–156.

Sasaki, A., Ishihara, S., 1979. Sulfur isotopic composition of the magnetite-series and ilmenite-series granitoids in Japan. Contrib. Mineral. Petrol. 68, 107–115.

Saunders, J.A., Mathur, R., Kamenov, G.D., Shimizu, T., Brueseke, M.E., 2016. New isotopic evidence bearing on bonanza (Au-Ag) epithermal ore-forming processes. Miner. Dep. 51, 1–11.

Seal, R.R., 2006. Sulfur isotope geochemistry of sulfide minerals. Rev. Mineral. Geochem. 61, 633–677.

Siyako, M., Burkan, K.A., Okay, A.I., 1989. Tertiary geology and hydrocarbon potential of the Biga and Gelibolu Peninsula. TAPG Bull. 1 (3), 183–199 (in Turkish with English abstract).

Stampfli, G.M., Borel, G.D., 2004. The TRANSMED transects in space and time: constraints on the paleotectonic evolution of the Mediterranean domain. In: Cavazza, W., Roure, F., Spakman, W., Stampfli, G.M., Ziegler, P. (Eds.), The TRANSMED Atlas: The Mediterranean Region from Crust to Mantle. Springer Verlag, Berlin, pp. 53–80.

Şengör, A.M.C., Satır, M., Akkök, R., 1984. Timing of tectonic events in the Menderes massif, western Turkey. Implications for tectonic evolution and evidence for Pan- African basement in Turkey. Tectonics 3, 693–707.

Şengör, A.M.C., Yılmaz, Y., 1981. Tethyan evolution of Turkey: a plate tectonic approach. Tectonophysics 75, 181–241.

Taylor, P.D.P., Maeck, R., De Bièvre, P., 1992. Determination of the absolute isotopic composition and atomic weight of a reference sample of natural iron. International Journal of Mass Spectrometry and Ion Processes 121, 111–125.

Ünal-İmer, E., Güleç, N., Kuşcu, I., Fallick, A.E., 2013. Genetic investigation and comparison of Kartaldağ and Madendağ epithermal gold deposits in Çanakkale. NW Turkey. Ore Geol. Rev. 53, 204–222.

Wang, D., Sun, X., Zheng, Y.Y., Wu, S., Xia, S.L., Chang, H.F., Yu, M., 2017. Two pulses of mineralization and genesis of the Zhaxikang Sb-Pb-Zn-Ag deposit in southern Tibet: Constraints from Fe-Zn isotopes. Ore Geol. Rev. 84, 347–363.

Wang, Y., Zhu, X.K., Cheng, Y., 2015. Fe isotope behaviours during sulfide-dominated skarn-type mineralisation. J. Asian Earth Sci. 103, 374–392.

Wang, Y., Zhu, X.K., Mao, J.W., Cheng, Y.B., Li, Z.H., 2014. Preliminary study on Cu isotopic geochemistry behavior of Dongguashan porphyry-skarn deposit. Tongling district. Acta Geol Sin 88, 2413–2422 (in Chinese with English abstract).

Wang, Y., Zhu, X.K., Mao, J.W., Li, Z.H., Cheng, Y.B., 2011. Iron isotope fractionation during skarn-type metallogeny: a case study of Xinqiao Cu-S-Fe-Au deposit in the Middle-Lower Yangtze valley. Ore Geol. Rev. 43, 194–202.

Wawryk, C.M., Foden, J.D., 2017. Iron-isotope systematics from the Batu Hijau Cu-Au deposit, Sumbawa. Indonesia. Chem. Geol. 466, 159–172.

Wilson, A.J., Cooke, D.R., Harper, B.J., Deyell, C.L., 2007. Sulfur isotopic zonation in the Cadia district, southeastern Australia: Exploration significance and implications for the genesis of alkalic porphyry gold-copper deposits. Miner. Depos. 42, 465–487.

Wu, L.Y., Hu, R.Z., Li, X.F., Liu, S.A., Tang, Y.W., Tang, Y.Y., 2017. Copper isotopic compositions of the Zijinshan high-sulfidation epithermal Cu-Au deposit, South China: Implications for deposit origin. Ore Geol. Rev. 83, 191–199.

Yao, J., Mathur, R., Sun, W., Song, W., Chen, H., Mutti, L., Luo, X., 2016. Fractionation of Cu and Mo isotopes caused by vapor-liquid partitioning, evidence from the Dahutang W-Cu-Mo ore field. Geochem. Geophys. Geosys. 17, 1725–1739.

Yenigün, K., 1978. The geological report of Alandere Pb-Zn-Cu mineralization in Çakır Village (Yenice/Çanakkale). Mineral Research and Exploration Institute of Turkey (MTA). Report 6564. Ankara (in Turkish, unpublished).

Yılmaz, H., Oyman, T., Sonmez, F.N., Arehart, G.B., Billor, Z., 2010. Intermediate sulfidation epithermal gold-base metal deposits in Tertiary subaerial volcanic rocks, Şahinli/Tespih Dere (Lapseki/Western Turkey). Ore Geol. Rev. 37, 236–258.

Yiğit, O., 2012. A prospective sector in the Tethyan Metallogenic Belt: geology and geochronology of mineral deposits in the Biga Peninsula. NW Turkey. Ore Geol. Rev. 46, 118–148.

Yücelay, M.A., 1971. Pb-Zn exploration around the Karaköy-Arapuçandere, Yenice-Çanakkale. Mineral Research and Exploration Institute of Turkey (MTA). Report No 4688. Ankara (in Turkish).

Yücelay, M.A., 1976. Geological report for drilling in the Karaköy Arapuçandere Pb-Zn- Cu mine area, Yenice-Çanakkale. Mineral Research and Exploration Institute of Turkey (MTA). Report No. 5655. Ankara (in Turkish).

Zartman, R.E., Doe, B.R., 1981. Plumbotectonics-the model. Tectonophysics 75, 135–162.

Zhu, B., Zhang, H.F., Zhao, X.M., He, Y.S., 2016. Iron isotope fractionation during skarn-type alteration: implications for metal source in the Han-Xing iron skarn deposit. Ore Geol. Rev. 74, 139–150.

Zhu, Z.Y., Jiang, S.Y., Mathur, R., Cook, N.J., Yang, T., Wang, M., Ma, L., Ciobanu, C.L., 2018. Iron isotope behavior during fluid/rock interaction in K-feldspar alteration zone - a model for pyrite in gold deposits from the Jiaodong Peninsula East China. Geochim. Cosmochim. Acta 222, 94–116.

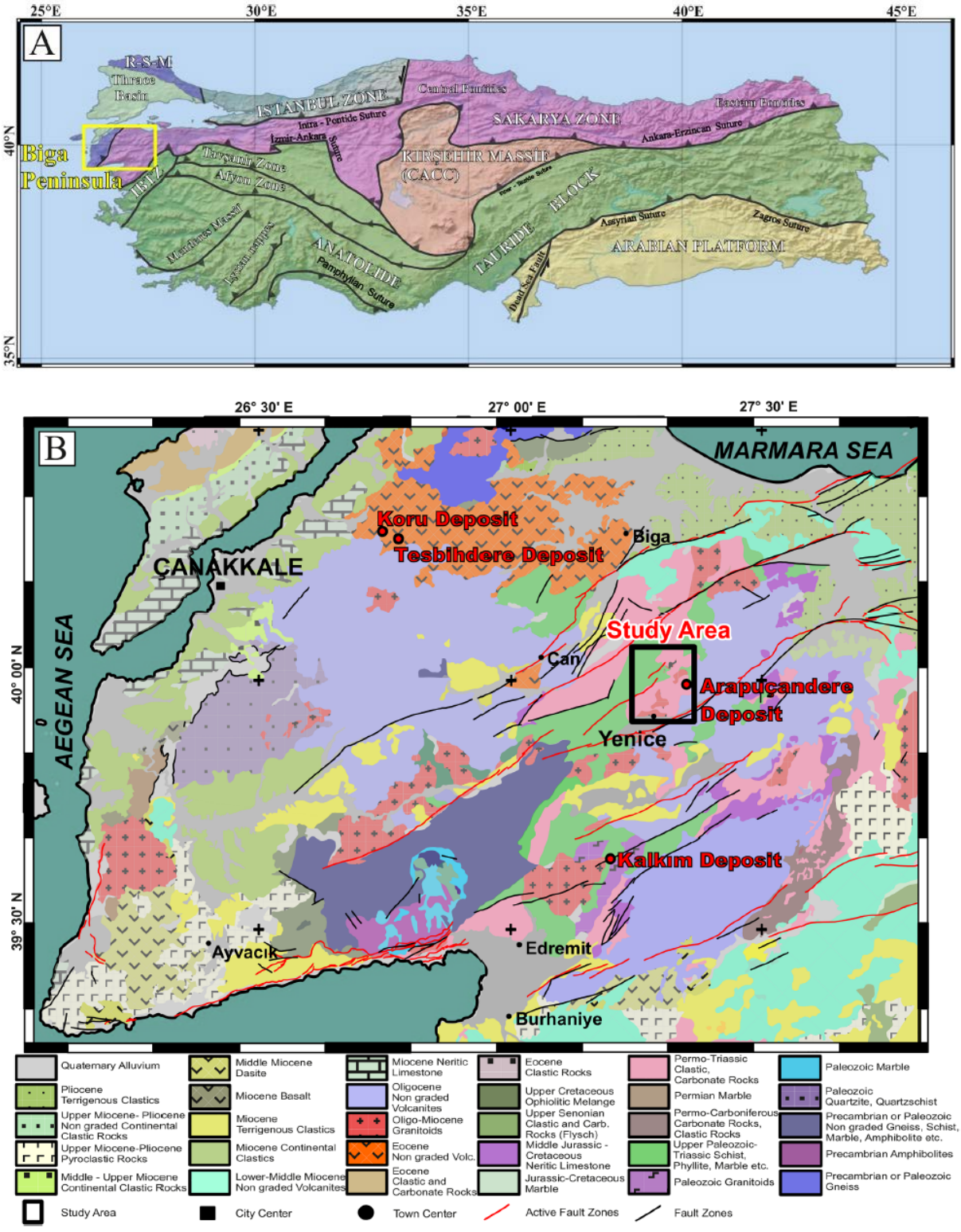

Fig. 1. (A) Tectonic framework of Turkey showing the major sutures and continental blocks (modified from Okay and Tüysüz, 1999), and (B) Simplified geological map of the Biga Peninsula (modified from Emre et al., 2013; Akbas¸ et al., 2017; Oyman, 2019).

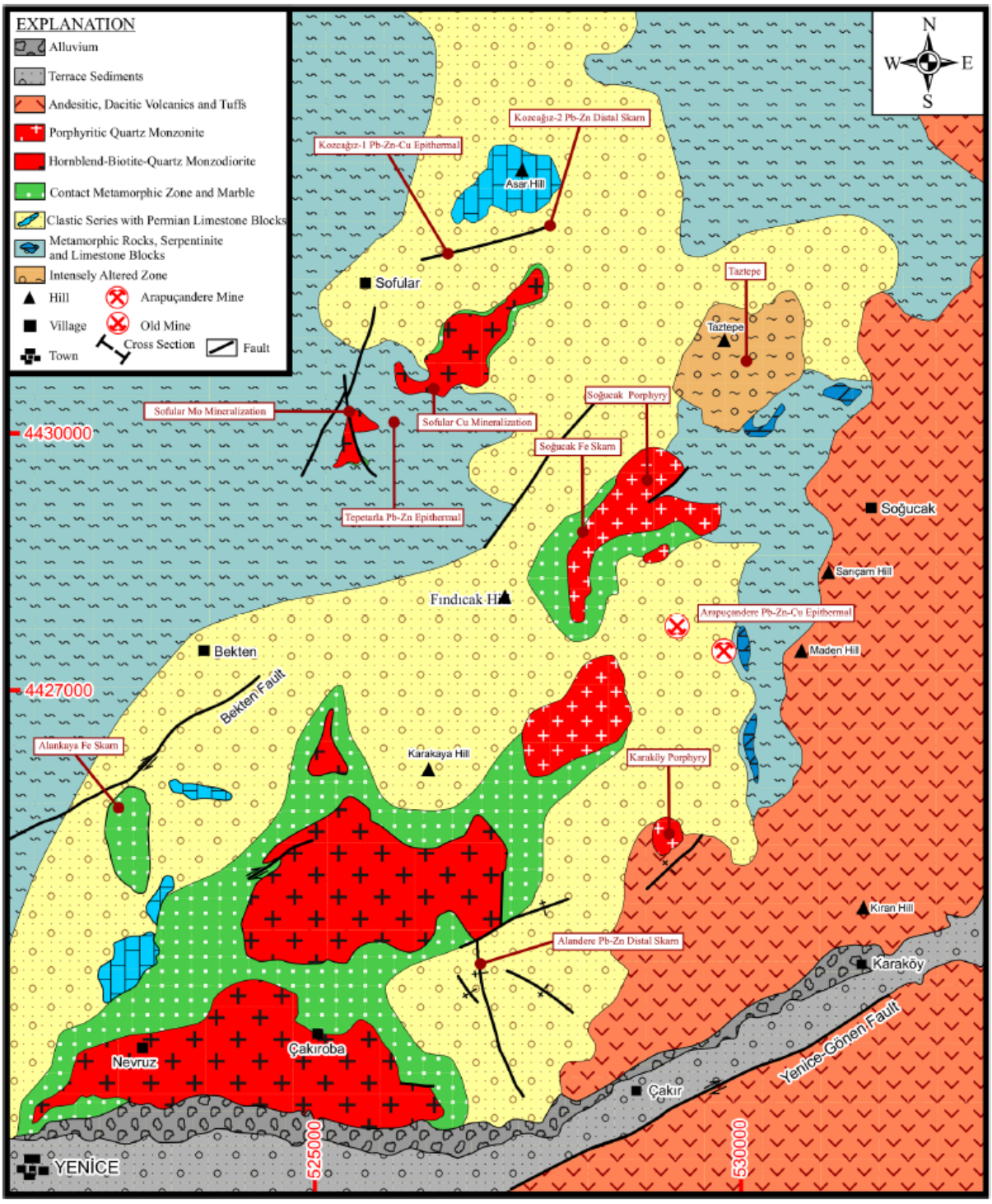

Fig. 2. Local geological map of the northeast of Yenice region (modified from Anıl, 1979; Öngen, 1982) with location of the various types of mineralization in the region.

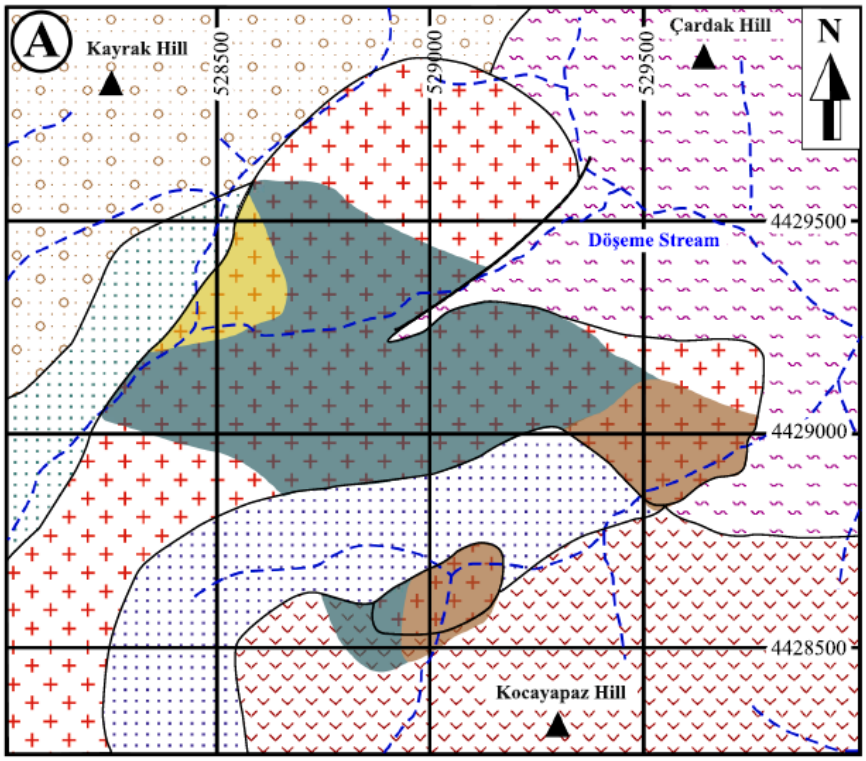

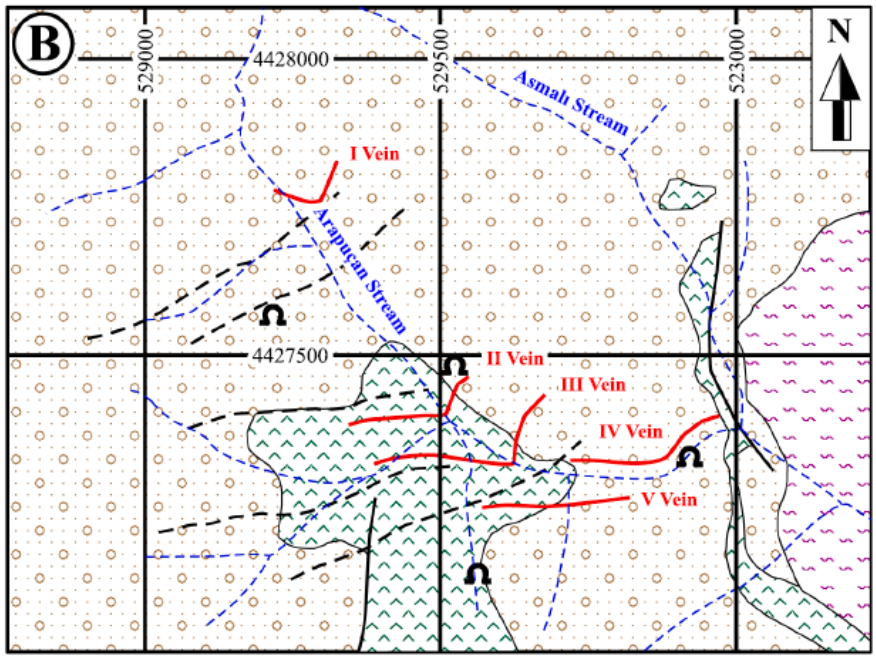

EXPLANATION

Oligocene
- Soğucak Porphyry
- Hallaçlar Volcanics

Triassic
- Metadiabase
- Metasandstone

Hodul Unit

Permian
- Schist-Phyllite, marble (Nilüfer Unit)

- Phyllic Zone
- Propylitic Zone
- Argillic Zone
- Skarn Zone
- Calc-Silicate Zone

- Mineralized vein
- Fault
- Mine entrance
- Hill
- Stream

Fig. 3. (A) Geology and alteration of the Soğucak porphyry and skarn. (B) Geological map of the Arapuçandere Pb-Zn-Cu ± Ag ± Au deposit showing the economically important veins in the area (modified from Yücelay, 1971; Bozkaya, et al., 2008).

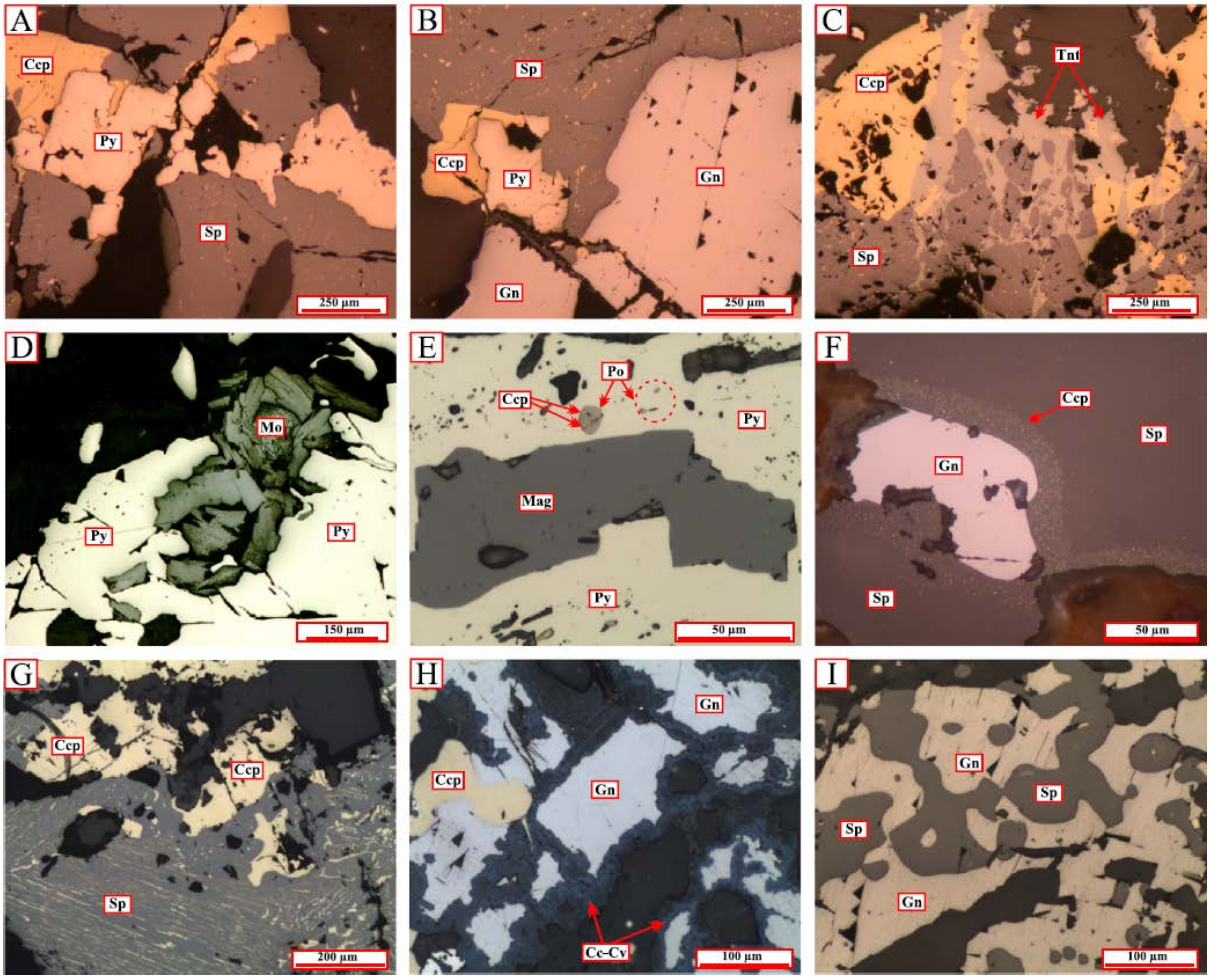

Fig. 4. Representative photomicrographs displaying ore textures and mineral associations in the various types of mineralization in the Yenice region (reflected plane-polarized light images). Arapuçandere deposit: (A and B) massive sulfide consisting of sphalerite, chalcopyrite, galena and pyrite, and (C) sulfides showing replacement by tennantite. Soğucak porphyry: (D) Molybdenite grains between euhedral to subhedral grains of pyrite. Soğucak skarn: (E) Subhedral magnetite in a fissure of pyrite and unorientated blebs of chalcopyrite and pyrrhotite within pyrite. Alandere mineralization: (F) Galena replaced by sphalerite and orientated exsolutions of chalcopyrite. Kozcağız-I mineralization: (G) Anhedral mass and orientated exsolutions of chalcopyrite within sphalerite, and (H) replacement of euhedral galena by chalcopyrite and chalcocite-covellite. Kozcağız-II mineralization: (I) Replacement of galena by sphalerite.

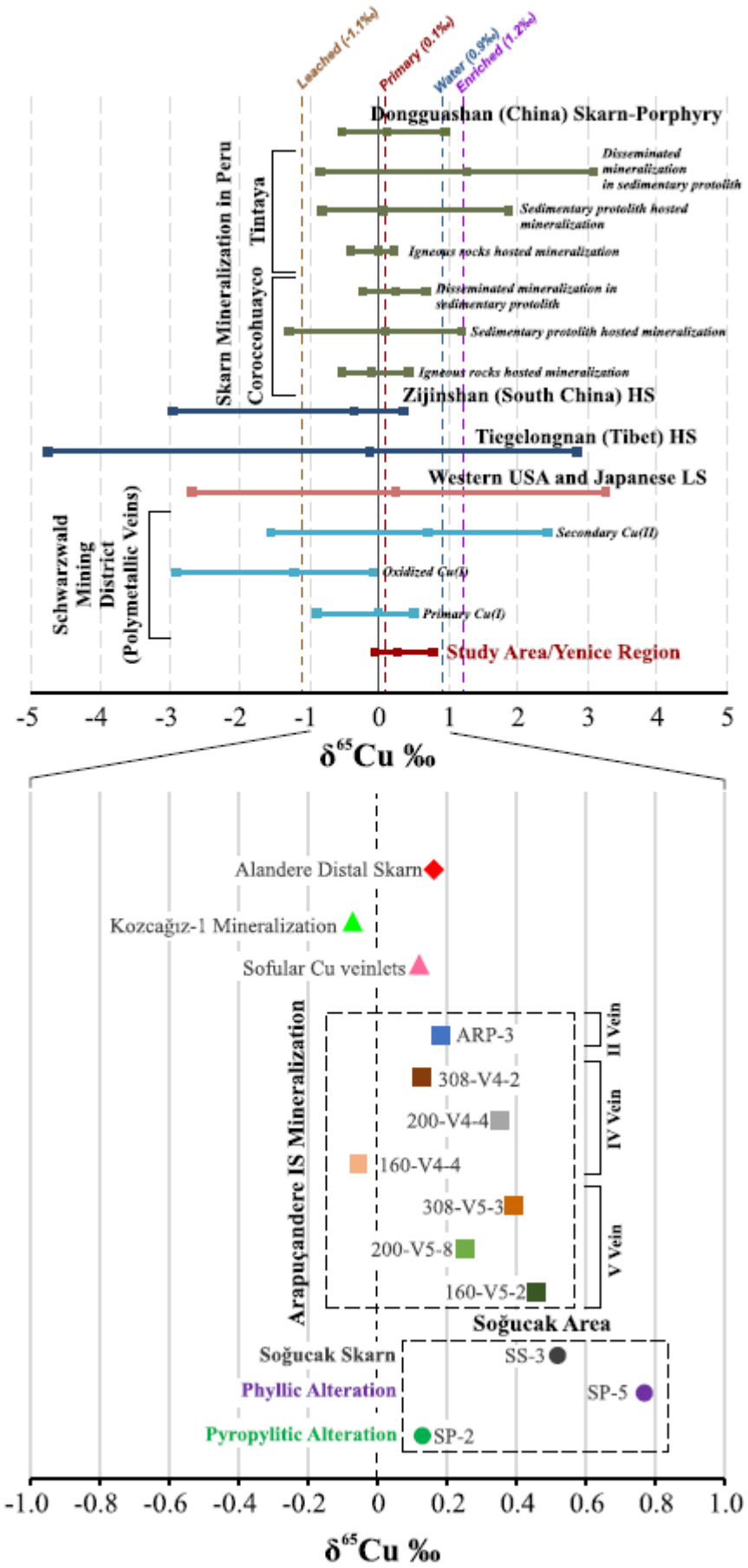
Leached (-1.1‰)
Primary (0.1‰)
Water (0.9‰)
Enriched (1.2‰)
Dongguashan (China) Skarn-Porphyry
Skarn Mineralization in Peru
Tintaya
Disseminated mineralization in sedimentary protolith
Sedimentary protolith hosted mineralization
Igneous rocks hosted mineralization
Coroccohuayco
Disseminated mineralization in sedimentary protolith
Sedimentary protolith hosted mineralization
Igneous rocks hosted mineralization
Zijinshan (South China) HS
Tiegelongnan (Tibet) HS
Western USA and Japanese LS
Schwarzwald Mining District (Polymetallic Veins)
Secondary Cu(II)
Oxidized Cu(I)
Primary Cu(I)
Study Area/Yenice Region
-5 -4 -3 -2 -1 0 1 2 3 4 5
δ65Cu ‰
Alandere Distal Skarn
Kozcağız-1 Mineralization
Sofular Cu veinlets
Arapuçandere IS Mineralization
ARP-3
308-V4-2
200-V4-4
160-V4-4
308-V5-3
200-V5-8
160-V5-2
II Vein
IV Vein
V Vein
Soğucak Area
Soğucak Skarn
SS-3
Phyllic Alteration
SP-5
Pyropylitic Alteration
SP-2
-1.0 -0.8 -0.6 -0.4 -0.2 0 0.2 0.4 0.6 0.8 1.0
δ65Cu ‰

Fig. 5. Cu isotopic compositions of pyrite and chalcopyrite from Soğucak porphyry-skarn, Arapuçandere deposit, Alandere distal skarn, Sofular-Cu and Kozcağız-I mineralization in the Yenice region. The dashed lines represent the average Cu isotopic compositions of the reservoirs in the ore deposit system (Mathur and Wang, 2019). Compilation of Cu isotope data from various hydrothermal ore deposits: Schwarzwald mining district (Markl et al., 2006a) in Germany, Western USA and Japanese low sulfidation deposits (Saunders et al., 2016), Tiegelongnan high sulfidation copper deposit (Duan et al., 2016) in Tibet, Zijinshan high sulfidation Cu-Au Deposit (Wu et al., 2017) in China, Coroccohuayco and Tintaya hypogene skarn mineralization (Maher and Larson, 2007) in Peru, and Dongguashan porphyry-skarn Cu-Au Deposit (Wang et al., 2014) in China.

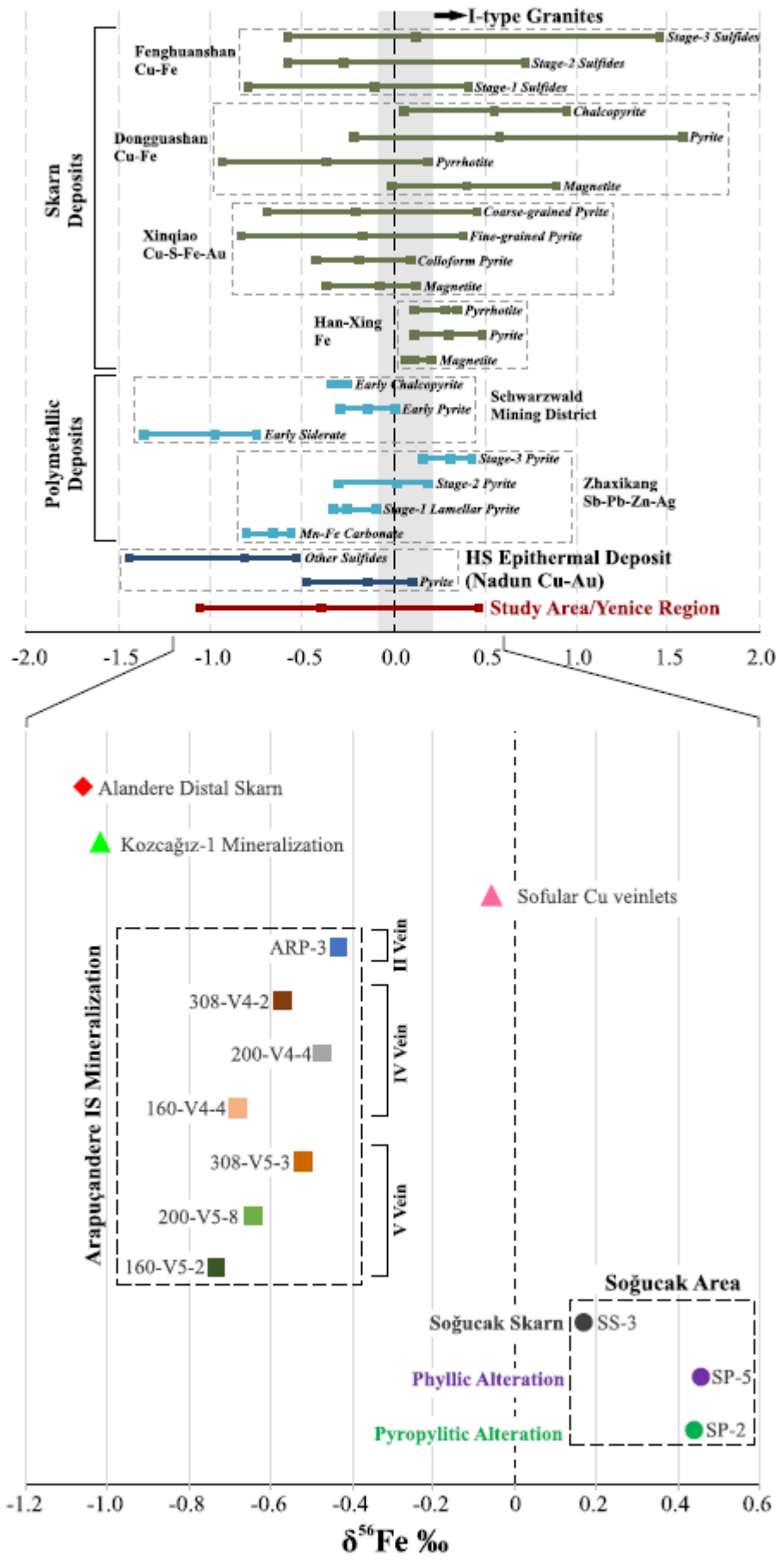
I-type Granites
Skarn Deposits
Fenghuanshan Cu-Fe
Stage-3 Sulfides
Stage-2 Sulfides
Stage-1 Sulfides
Dongguashan Cu-Fe
Chalcopyrite
Pyrite
Pyrrhotite
Magnetite
Xinqiao Cu-S-Fe-Au
Coarse-grained Pyrite
Fine-grained Pyrite
Colloform Pyrite
Magnetite
Han-Xing Fe
Pyrrhotite
Pyrite
Magnetite
Polymetallic Deposits
Early Chalcopyrite
Early Pyrite
Schwarzwald Mining District
Early Siderate
Stage-3 Pyrite
Stage-2 Pyrite
Zhaxikang Sb-Pb-Zn-Ag
Stage-1 Lamellar Pyrite
Mn-Fe Carbonate
Other Sulfides
HS Epithermal Deposit (Nadun Cu-Au)
Pyrite
Study Area/Yenice Region
-2.0
-1.5
-1.0
-0.5
0.0
0.5
1.0
1.5
2.0
Alandere Distal Skarn
Kozcağız-1 Mineralization
Sofular Cu veinlets
Arapuçandere IS Mineralization
ARP-3
II Vein
308-V4-2
200-V4-4
IV Vein
160-V4-4
308-V5-3
200-V5-8
V Vein
160-V5-2
Soğucak Area
Soğucak Skarn
SS-3
Phyllic Alteration
SP-5
Pyropylitic Alteration
SP-2
-1.2
-1.0
-0.8
-0.6
-0.4
-0.2
0
0.2
0.4
0.6
δ56Fe ‰

Fig. 6. Fe isotopic compositions of pyrite and chalcopyrite from Soğucak porphyry-skarn, Arapuçandere deposit, Alandere distal skarn, Sofular-Cu and Kozcağız-I mineralization in the Yenice region. The shaded area corresponds to the Fe isotopic compositions of I-type granites (Foden et al., 2015 and references therein). Compilation of Fe isotope data from various hydrothermal ore deposits: Nadun Cu-Au deposit (Li et al., 2016) and Zhaxikang Sb-Pb-Zn-Ag deposit (Wang et al., 2017) in Tibet, Schwarzwald mining district (Markl et al., 2006b) in Germany, Han-Xing Fe deposit (Zhu et al., 2016), Xingiao Cu-S-Fe-Au deposit (Wang et al., 2011), Dongguashan and Fenghuanshan Cu-Fe deposits (Wang et al., 2015) in China.

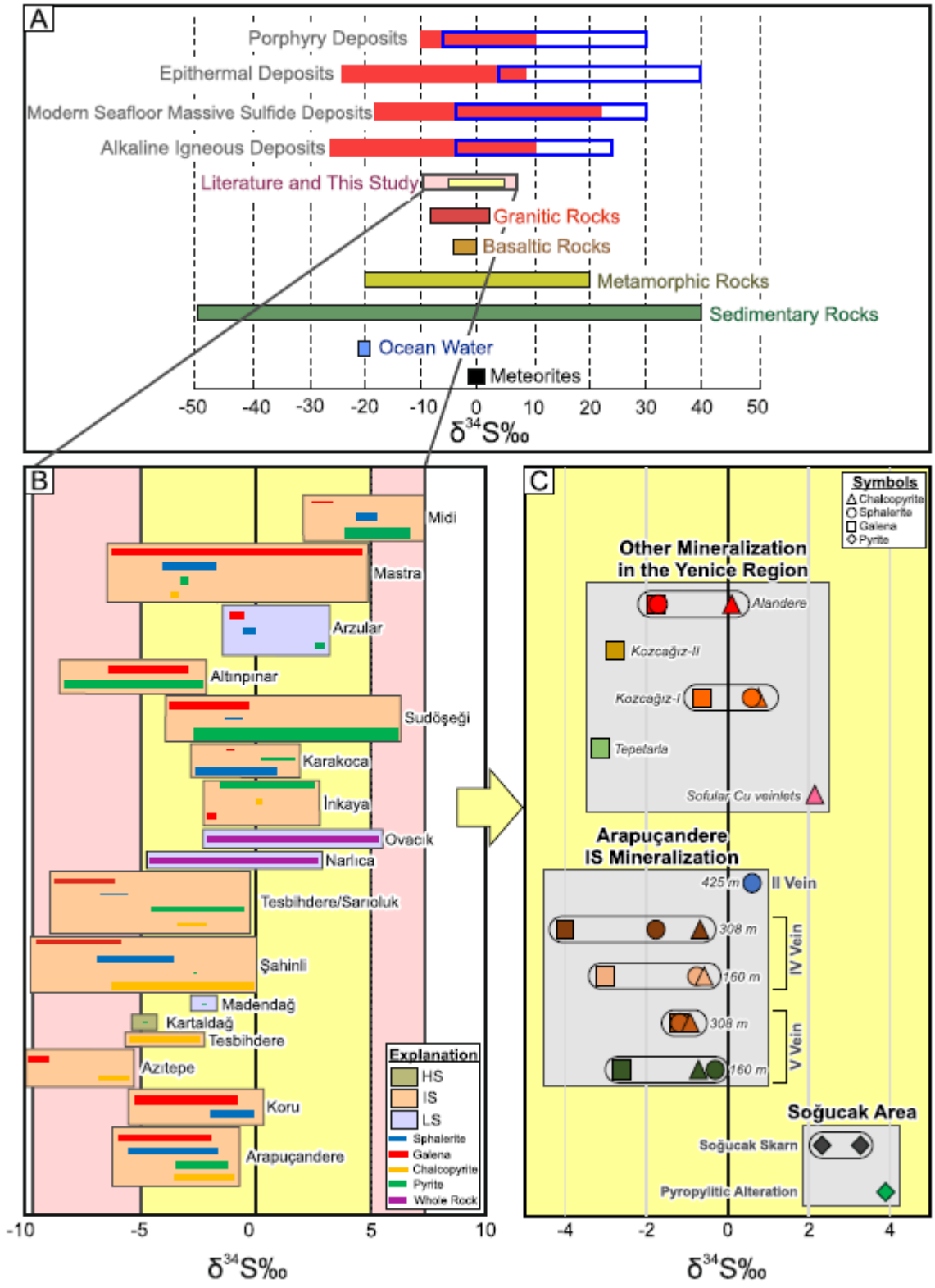

Fig. 7. $\delta^{34}S$ values for the mineralization in the Yenice region compared with those of ore systems, important sulfur reservoirs (A) and epithermal deposits in the Biga Peninsula (B), and range of $\delta^{34}S$ values for sulfides from the various types of mineralization Yenice region (C). The red filled and blue outlined bars in the ore systems correspond to $\delta^{34}S$ values of sulfide and sulfate, respectively. Compilation of S isotope data: Ore systems from Hutchison et al.

(2020), sulfur reservoirs from Hoefs (2009), and epithermal deposits in Biga Peninsula from Oyman (2019) and references therein.

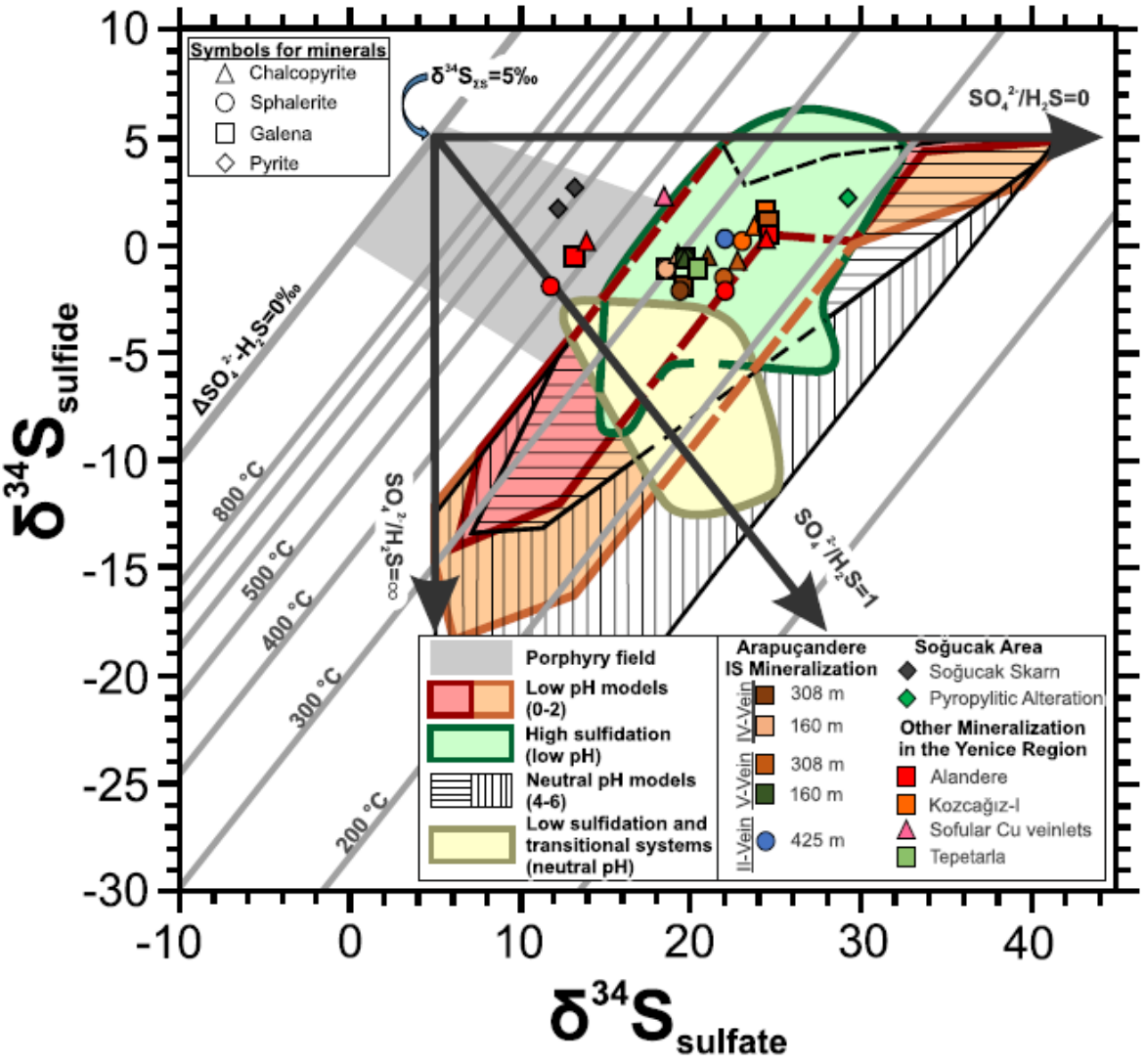

Fig. 8. $\delta^{34}S_{sulfate}$-$\delta^{34}S_{sulfide}$ diagram of the mineralization in the Yenice region (after Fifarek and Rye, 2005). Fields for hydrothermal ore deposits and pH models are from Hutchison et al. (2020). The gray lines represent equivalent temperatures that were calculated from equilibrium fractionation factors of Ohmoto and Lasaga (1982).

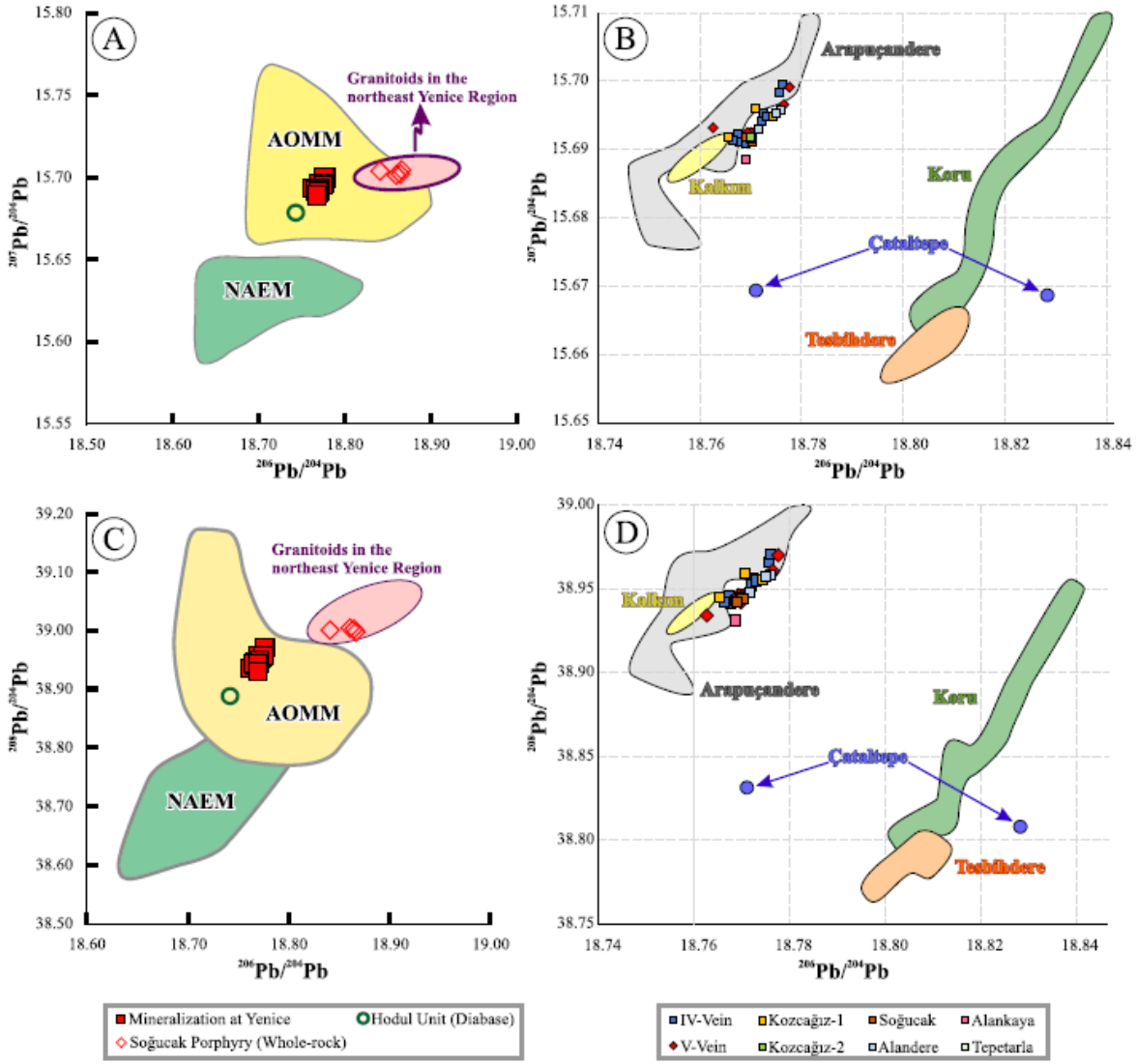

Fig. 9. Lead isotope evolution diagrams of galena, pyrite, chalcopyrite and magnetite from mineralization in the Yenice region: (A) $^{207}Pb/^{204}Pb$ vs $^{206}Pb/^{204}Pb$ and (C) $^{208}Pb/^{204}Pb$ vs $^{206}Pb/^{204}Pb$ compared with data from NAEM: North Anatolian Eocene Magmatic rocks and AOMM: Aegean to West Anatolian Oligocene-Miocene Magmatic rocks (Marchev et al., 2004; Chakrabarti et al., 2012; Altunkaynak and Dilek, 2013; Gülmez et al., 2013; Ersoy and Palmer, 2013), and (B) $^{207}Pb/^{204}Pb$ vs $^{206}Pb/^{204}Pb$ and (D) $^{208}Pb/^{204}Pb$ vs $^{206}Pb/^{204}Pb$ compared with the data from Arapuçandere (Bozkaya, 2011), Çataltepe (Demirela, 2011), Koru (Bozkaya and Gökçe, 2009; Çiçek and Oyman, 2016), Tesbihdere (Çiçek and Oyman, 2016) and Kalkım mineralization (Akıska et al., 2013) in Biga Peninsula.

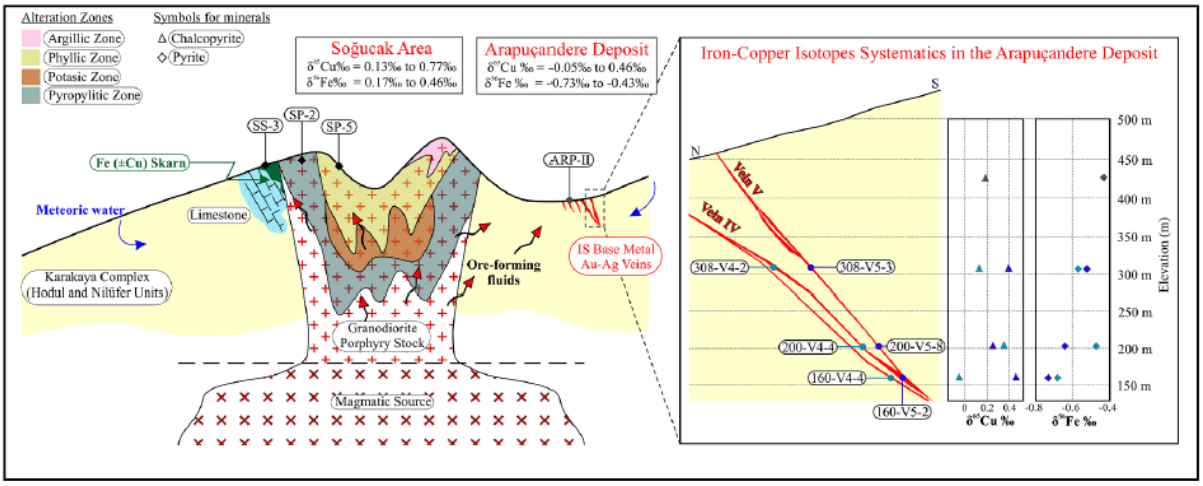

Fig. 10. Schematic cross section through Soğucak area and Arapuçandere deposit (non-scaled), showing the hydrothermal mineralization, alteration zoning and generalized fluid paths, Fe and Cu isotope ranges measured from the Yenice region. Sample locations and Fe-Cu isotope patterns for the IV and V veins at Arapuçandere deposit are also shown in the right box.

Table 1 Detailed descriptions of the samples used for isotopic analysis from various types of mineralization in the Yenice region.

Mineralization		Sample Number	Elevation (m)	Mineral Assemblage – Ore Type
Arapuçandere Deposit	II-Vein	ARP-3	425	Sp-Gn-rich ore with less abundant Ccp in the coarse crystalline amethyst vein at the surface
	IV-Vein	KA-4	360	Base metal sulfides bearing banded Qz vein within silicified diabase at the surface
		160-V4-1	160	Gn-rich ore zone with less abundant Ccp > Sp > Py > Ag, and Cal ± Qz as gangue minerals
		160-V4-4	160	Gn-rich ore zone with less abundant Ccp > Sp > Py > Ag, and Cal ± Qz as gangue minerals
		160-V4-9	160	Gn-Sp-rich ore zone with less abundant Ccp > Py > Ag, and Cal ± Qz as gangue minerals
		240-V4-1	240	Gn-rich ore zone with less abundant Sp > Ccp > Py > Ag, and Qz ± Cal as gangue minerals
		308-V4-1	308	Gn-rich ore zone with less abundant Sp > Ccp > Py > Ag, and Qz ± Cal as gangue minerals
	V-Vein	160-V5-1	160	Gn-Ccp-rich ore zone with less abundant Sp > Py > Ag, and Cal ± Qz as gangue minerals
		160-V5-3	160	Gn-Ccp-rich ore zone with less abundant Sp > Py > Ag > Au, and Cal ± Qz as gangue minerals
		200-V5-7	200	Gn-rich ore zone with less abundant Ccp > Sp > Py > Ag > Au, and Qz > Cal as gangue minerals
		200-V5-8	200	Gn-Sp-rich ore zone with less abundant Ccp > Py > Ag, and Qz > Cal as gangue minerals
		308-V5-3	308	Gn-rich ore zone with less abundant Sp > Ccp > Py, and Cal ± Qz as gangue minerals
Alandere		ÇK-1 ÇK-2 ÇK-3 ÇK-4	341 345 346 344	Medium to fine-grained Gn-Sp- Ccp-Py-Hem bearing distal skarn vein zones: (1) Fine-grained Gn-Sp ore with minor Py in Cal > Grt skarn zone, (2) Fine-grained Ccp-Hem-Py ore in Amp > Qz-Cal > Prx skarn zone, (3) Medium-grained Gn-Sp-Ccp-Py ore in Amp > Grt > Cal-Qz skarn Sp ore with minor Hem-Ccp-Py in Amp > Grt > Qz > Cal > Prx skarn zone
Alankaya		TS-3	400	Irregular massive Fe ± Cu ore containing medium-grained Mag-Ccp-Hem-Po in Grt- Prx > Amp-Ep skarn zone
Sofular Cu		SG-4	345	Medium-grained Ccp bearing intraplutonic Qz vein within Sofular intrusion
Kozcağız-I		SR-V1-A SR-V1-B SR-V1-C SR-V1-E	303	Coarse to medium-grained Gn- Sp-Ccp-(Py-Apy) bearing Qz vein zones: (A) Gn-Sp-Ccp ore, (B) Sp-Gn-Ccp ore with minor Py, (C) Gn-Sp-Ccp breccia ore, and (E) Gn-Sp-Ccp ore with minor Py-Apy
Kozcağız-II		SR-S-4	332	Hornfels-hosted disseminated medium to fine-grained Gn-Sp and minor Ccp
Tepetarla		KKY-19	331	Medium-grained Gn with minor Sp-Ccp-Qtz in massive ore
Soğucak Porphyry		SP-1	476	Less altered porphyry containing Plj-Kfs-Amp-Qz-Bt with minor disseminated Mag
		SP-2	499	Moderately altered porphyry (inner pyropylitic alteration) containing Amp-Plj-Kfs-Qz-Bt with Ep-Car-Chl-Mag-Py alteration assemblages
		SP-5	500	Most intensively altered porphyry (phyllic alteration) containing Qz-Ser-Chl-Py

	AC-13	422	Less altered porphyry containing Plj-Kfs-Amp-Qz-Bt with minor disseminated Mag
	AC-14	496	Less altered porphyry containing Plj-Kfs-Amp-Qz-Bt with minor disseminated Mag- Py
Soğucak Skarn	SS-3	554	Medium to fine-grained Mag- Py ore with sparsely disseminated Ccp in Grt > Cpx skarn zone
	SS-6–2	533	Coarse-grained Py-rich ore with Mag-Ccp in Grt > Cpx > Ep > Amp skarn zone
	SS-6–3		Medium to fine-grained Mag-rich ore with Py-Ccp in Grt > Cpx > Ep > Amp skarn zone

Table 2 Copper and iron isotopic compositions of pyrite and chalcopyrite from various types of mineralization in the Yenice region.

Mineralization		Sample No	Mineral	δ^{65}Cu ‰	δ^{57}Fe ‰	δ^{56}Fe ‰
Arapuçandere Deposit	II-Vein	ARP-3	Chalcopyrite	0.18		
			Pyrite		-0.63	-0.43
	IV-Vein	160-V4-4	Chalcopyrite	-0.05		
			Pyrite		-0.99	-0.68
		200-V4-4	Chalcopyrite	0.35		
			Pyrite		-0.71	-0.47
		308-V4-2	Chalcopyrite	0.13		
			Pyrite		-0.86	-0.57
	V-Vein	160-V5-2	Chalcopyrite	0.46		
			Pyrite		-1.04	-0.73
		200-V5- 8	Chalcopyrite	0.25		
			Pyrite		-0.93	-0.64
		308-V5-3	Chalcopyrite	0.39		
			Pyrite		-0.75	-0.52
Alandere		ÇK-2	Chalcopyrite	0.16	-1.41	-1.06
Sofular Cu		SG-4	Chalcopyrite	0.12	-0.07	-0.06
Kozcağız-I		SR-V1-C	Chalcopyrite	-0.07	-1.41	-1.02
Soğucak Porphyry		SP-2	Pyrite	0.13	0.71	0.44
		SP-5	Pyrite	0.77	0.66	0.46
Soğucak Skarn		SS-3	Pyrite	0.52	0.23	0.17

Table 3 Sulfur isotopic compositions of galena, pyrite, chalcopyrite, sphalerite from various 6 types of mineralization in the Yenice region. The $\delta^{34}S$ values of H_2S_{aq} in equilibrium with the 7 sulfides were calculated by using average homogenization temperatures of fluid inclusions for 8 each mineralization, with the exception of the Alandere mineralization temperatures that were 9 estimated using the temperature range of mineral chemistry geothermometry determined by 10 previous studies of Çiçek et al. (2017a), Çiçek et al. (2017b) and Çiçek and Oyman (2018), Çiçek and Oyman (2019a), Çiçek and Oyman (2019b).

Mineralization		Sample No	$\delta^{34}S$-Sulfides (‰)				$\delta^{34}S$-H_2S (‰)[a]				Temperature[b] (◦C)
			Galena	Sphalerite	Chalcopyrite	Pyrite	Galena	Sphalerite	Chalcopyrite	Pyrite	
Arapuçandere Deposit	II-Vein	ARP-3		0.6			0.3				
	IV-Vein	160-V4-9	-3.0	-0.8	-0.6		-1.1	-1.1	-0.4		295.9
		308-V4-1	-4.0	-1.8	-0.7		-1.9	-2.1	-0.5		297.8
	V-Vein	160-V5-3	-2.6	-0.3	-0.7		-0.6	-0.6	-0.6		292.3
		308-V5-3	-1.2	-1.2	-0.9		1.1	-1.5	-0.7		Not equilibrated
Alandere		ÇK-2							0.2 to 0.3		
		ÇK-4	-1.8	-1.7			-0.5 to 0.5	-2.1 to -1.9			Not equilibrated
Sofular Cu		SG-4							2.3		
Tepetarla		KKY-19	-3.1				-1.1				
Kozcağız-I		SR-V1A	-0.6	0.6	0.8		1.6	0.2	0.9		Not equilibrated
Kozcağız-II		SR-S-4	-2.7								
Soğucak Porphyry		SP-2				3.9				2.2	
Soğucak Skarn		SS-3				3.3				2.7	
		SS-6				2.3				1.7	

a $\delta^{34}S$ values of H_2S_{aq} in equilibrium with the sulfides calculated from the equations of Ohmoto and Rye (1979). b Temperature calculated from sphalerite-galena pair on the based of equilibrium isotopic fractionation factors of Ohmoto and Rye (1979).

Table 4 Lead isotope ratios of galena, pyrite, chalcopyrite, magnetite and whole-rock from various types of mineralization in the Yenice region.

Mineralization		Mineral	Sample No	$^{206}Pb/^{204}Pb$	$^{207}Pb/^{204}Pb$	$^{208}Pb/^{204}Pb$
Arapuçandere Deposit	IV-Vein	Galena	KA-4	18.7679	15.6911	38.9411
		Galena	160-V4-1	18.7675	15.6924	38.9459
		Galena	160-V4-2	18.7758	15.6983	38.9658
		Galena	160-V4-4	18.7723	15.6954	38.9552
		Galena	160-V4-9	18.7721	15.6942	38.9514
		Galena	200-V4-4	18.7703	15.6926	38.9468
		Galena	240-V4-1	18.7763	15.6994	38.9700
		Galena	275-V4-1	18.7666	15.6913	38.9420
		Galena	308-V4-1	18.7732	15.6948	38.9547
		Galena	308-V4-2	18.7690	15.6909	38.9421
	V-Vein	Galena	160-V5-1	18.7626	15.6932	38.9343
		Galena	160-V5-2	18.7701	15.6925	38.9455
		Galena	160-V5-3	18.7693	15.6925	38.9460
		Galena	200-V5-7	18.7776	15.6992	38.9698
		Galena	200-V5-8	18.7765	15.6966	38.9608
		Galena	308-V5-3	18.7697	15.6913	38.9418
Kozcağız-I		Galena	SR-V1-A	18.7744	15.6948	38.9550
		Galena	SR-V1-B	18.7655	15.6919	38.9450
		Galena	SR-V1-E	18.7708	15.6961	38.9584
Kozcaız-II		Galena	SR-S-4	18.7699	15.6918	38.9445
Alandere		Galena	ÇK-1	18.7761	15.6957	38.9572
		Chalcopyrite	ÇK-3	18.7751	15.6953	38.9569
		Galena	ÇK-4	18.7717	15.6930	38.9479
Tepetarla		Galena	KKY-19	18.7698	15.6916	38.9436
Soğucak Skarn		Pyrite	SS-3	18.7704	15.6912	38.9434
		Pyrite	SS-6–2	18.7691	15.6919	38.9418
Alankaya		Magnetite	TS-3	18.7690	15.6886	38.9305
Soğucak Porphyry (Whole-Rock)		Less altered	SP-1	18.8669	15.7041	38.9984
		Prophylitic	SP-2	18.8612	15.7015	39.0045

		Less altered	AC-13	18.8412	15.7037	39.0012
		Less altered	AC-14	18.8654	15.7020	39.0023